DTIC FILE COPY

Unclassified

SECURITY CLASSIFICATION OF THIS PAGE (When Data Entered)

REPORT DOCUMENTATION PAGE		READ INSTRUCTIONS BEFORE COMPLETING FORM
1. REPORT NUMBER AFOSR-TR- 88-0632	2. GOVT ACCESSION NO.	3. RECIPIENT'S CATALOG NUMBER
4. TITLE (and Subtitle) Computer Aided Design of Monolithic Microwave and Millimeter Wave Integrated Circuits and Subsystems		5. TYPE OF REPORT & PERIOD COVERED Final Technical Report 6. PERFORMING ORG. REPORT NUMBER 01Sep 84 - 31 Dec 86
7. AUTHOR(s) Walter H. Ku, Guan-Wu Wang, J.Q. He and I. Ichitsubo		8. CONTRACT OR GRANT NUMBER(s) AFOSR Grant # AFOSR-84-0345
PERFORMING ORGANIZATION NAME AND ADDRESS Cornell University (Phillips Hall) School of Electrical Engineering Ithaca, N.Y. 14853		10. PROGRAM ELEMENT, PROJECT, TASK AREA & WORK UNIT NUMBERS 61102F 2305 C1
CONTROLLING OFFICE NAME AND ADDRESS AFOSR/NE Bolling Air Force Base, D.C. 20332 (Dr. Gerald Witt)		12. REPORT DATE 13. NUMBER OF PAGES
MONITORING AGENCY NAME & ADDRESS(if different from Controlling Office) AFOSR/NE Bolling AFB, DC 20332		15. SECURITY CLASS. (of this report) Unclassified 15a. DECLASSIFICATION/DOWNGRADING SCHEDULE

AD-A196 760

DISTRIBUTION STATEMENT (of this Report)

Approved for public release; distribution unlimited.

DTIC ELECTE JUL 01 1988 S D E

17. DISTRIBUTION STATEMENT (of the abstract entered in Block 20, if different from Report)

18. SUPPLEMENTARY NOTES

19. KEY WORDS (Continue on reverse side if necessary and identify by block number)

GaAs MESFETs, HEMTs, MODFETs, Monolithic Microwave and Millimeter Integrated Circuits, MMIC, MIMIC, Computer Aided Design, Large-Signal Device Models.

20. ABSTRACT (Continue on reverse side if necessary and identify by block number)

This final technical report presents results on the computer aided design of monolithic microwave and millimeter wave integrated circuits and subsystems. New results include analytical and computer aided device models of GaAs MESFETs and HEMTs or MODFETs, new synthesis techniques for monolithic feedback and distributed amplifiers and a new nonlinear CAD program for MIMIC called CADNON. This program incorporates the new MESFET and HEMT model and has been successfully applied to the design of monolithic millimeter-wave mixers.

DD FORM 1 JAN 73 1473 EDITION OF 1 NOV 65 IS OBSOLETE

S/N 0102-LF-014-6601

Unclassified

SECURITY CLASSIFICATION OF THIS PAGE (When Data Entered)

88 09 12

COMPUTER AIDED DESIGN OF MONOLITHIC MICROWAVE AND MILLIMETER WAVE INTEGRATED CIRCUITS AND SUBSYSTEMS

W.H. Ku, G-W. Wang, J.Q. He and I. Ichitsubo

Cornell University
School of Electrical Engineering and
National Submicron Facility
Phillips Hall
Ithaca, N.Y. 14853

DTIC COPY INSPECTED 6

May 1988

AFOSR Grant No. AFOSR-84-0345
Final Technical Report
September 1, 1985 through December 31, 1986

U.S. AIR FORCE OFFICE OF SCIENTIFIC RESEARCH
Bolling Air Force Base, D.C. 20332

COMPUTER AIDED DESIGN OF MONOLITHIC MICROWAVE AND MILLIMETER WAVE INTEGRATED CIRCUITS AND SUBSYSTEMS

ABSTRACT

This final technical report presents results of research on the computer aided design of monolithic microwave and millimeter wave integrated circuits and subsystems. New results include analytical and computer aided device models of the GaAs MESFETs and HEMTs or MODFETs, new synthesis techniques for monolithic feedback and distributed amplifiers and a new nonlinear CAD program for MIMIC called CADNON. This program incorporates the new MESFET and HEMT model and has been successfully applied to the design of monolithic millimeter-wave mixers.

TABLE OF CONTENTS

1. INTRODUCTION

This research program is concerned with the study and development of integrated computer aided design (CAD) of monolithic microwave and millimeter integrated circuits (MIMIC) and subsystems. It involves computer aided device modeling of submicron GaAs MESFETs and MISFETs, high electron mobility transistors (HEMTs) and heterojunction bipolar transistors (HBTs) and integrated CAD of analog and digital ICs using these submicron solid-state devices. The main tasks of this program are to:

1. Develop computer aided synthesis and design (CAS/CAD) techniques for analog linear MMIC. CAS/CAD techniques for MMIC/M^3IC will include ultra broadband monolithic circuits such as distributed amplifiers and direct-coupled feedback amplifiers using 0.25 μm GaAs MESFETs and HEMTs.
2. Develop computer aided design tools for integrated design packages for nonlinear MMIC/M^3ICs including mixers, frequency doublers and phase shifters. Emphasis will again be placed on ultra broadband monolithic circuits requiring systematic CAD software packages. Large-signal characterizations of the active solid-state 3-terminal devices (GaAs MESFETs, HEMTs and HBTs) and nonlinear circuit analysis program recently developed in this research program will form an integrated CAD package for MIMIC.
3. Develop process modeling for both analog and digital monolithic HEMT ICs.

Under the current AFOSR program, we have obtained the following results:

- We have successfully developed an analytical and computer aided model of the AlGaAs/GaAs HEMT. Results of this model have been published recently in the May 1986 issue of the IEEE Transactions on Electron Devices.
- We have applied the CAD programs for the designs of ultra-wideband monolithic amplifiers using 0.25 μm HEMT. One of these amplifiers has been fabricated by TRW.
- We have used the *nonlinear large-signal* CAD program developed under the AFOSR program for the design of monolithic GaAs mixers. It is believed that this is a major contribution to the design of MMIC/M^3IC. Currently available CAD programs are restricted to *linear* circuits.
- Recently, we have also completed the design of a monolithic direct-coupled feedback amplifier using submicron GaAs MESFETs. The results have been published in *IEEE Transactions on Microwave Theory and Techniques*, April 1987.

2. HETEROJUNCTION GaAs DEVICES

A number of new devices based on GaAs technology and molecular-beam epitaxy (MBE) material are emerging for ultra high-speed and high-frequency applications. Two of the most promising are the high electron mobility transistors (HEMT) or MODFET and the heterojunction bipolar transistors (HBT). Ultra high-speed integrated circuits with HEMT have demonstrated propagation delay per gate as low as 10 ps at room temperature. This result represents the highest speed ever reported for any solid-state device. Impressive results of analog HEMT's used for low noise microwave and millimeter applications have been reported. For a 0.25 μm gate-length HEMT, significant amplifier gain with associated low-noise performance has been demonstrated at frequencies as high as 60 GHz.

Impressive experimental results on digital HBT's and analog HBT's have also been reported using MBE grown material. Frequency dividers using HBT have reached frequencies as high as 10 GHz and analog HBT has demonstrated microwave performance above 10 GHz range. Our proposed investigation includes the study of three submicron devices: (1) high electron mobility transistors, (2) double heterojunction high electron mobility transistors and (3) heterojunction bipolar transistors. These devices will be used.

2.1 High Electron Mobility Transistors

High electron mobility or modulation doped transistors make use of enhanced mobility behavior first reported by Dingle et.al. Mobility enhancement was attributed to the spatial-separation between the electrons and their parent donor impurities, thereby reducing the influence of impurity scattering on the electron motion.

The significant improvements of HEMT results from utilization of a device structure based on properties of the GaAs-GaAlAs heterostructures and the accumulation of a two-dimensional electron gas (2DEG) at its interface. Due to the differences in bandgap and electron affinity in a lattice matched heterostructure system such as GaAs-GaAlAs, the electrons ionized from the donor impurities in the wider-bandgap semiconductor move to the narrow-bandgap semiconductor and accumulate in the potential well at the heterojunction interface. Because of the confinement of the carriers in this narrow (~ 100 Å or less) region, their freedom of motion is limited to two dimensions, and the carriers can be treated as a two-dimensional electron gas. If the narrow bandgap semiconductor is undoped or has very high purity, the carriers in the 2DEG suffer very little ionized impurity scattering which result in very high electron mobility.

With the recent advances in the epitaxial growth technology based on molecular beam, epitaxy (MBE), extremely high quality modulation doped structures can be achieved; electron mobilities in excess of 8,000 cm /V-s at 300K, 100,000 cm /V-s at 77 K and 200,000 cm /V-s at 10 K have been demonstrated. material technology based on metalorganic chemical vapor deposition (MOCVD) has also been successfully used for modulation doped structures.

The use of a modulation doped structure for device fabrication was first reported by Mimura et.al. in 1980. This device was similar to a field effect transistor but with the Schottky gate fabricated on the GaAlAs layer. Because of the mobility enhancement in this structure, this device has been described as a High Electron Mobility Transistor (HEMT). Although the structure of a HEMT is quite similar to that of a conventional MESFET, the operation is quite different. The conducting carriers are confined to a potential well at a fixed distance from the gate. Therefore, the operation of a HEMT is similar to that of a MOSFET in which the carriers are confined to the oxide-semiconductor interface. HEMT devices have shown very high transconductances and, because of the MOSFET-like charge control mechanism, they also shown

a high degree of linearity (i.e., the transconductance is constant over a very wide gate voltage range).

2.2 Double Heterojunction High Electron Mobility Transistors

A double heterojunction (DH) high electron mobility transistor (HEMT) structure consists of a heterojunction on both sides of the undoped GaAs channel. In a regular single heterojunction (SH) HEMT, the maximum number of electrons in the two dimensional electron gas (2DEG) at the interface potential well is about 1*10 cm, which is limited by the doping concentration and the Al content of the N-GaAlAs layer. Ideally, one would like to have this value as high as possible so that the device can have high transconductance over a wide gate voltage.

Recently, successful fabrication of DH HEMT's has been reported by Inoue and Sasaki of the University of Tokyo. More recently, Sheng, Lee et.al., of Rockwell have successfully fabricated DH HEMT's and obtained an extremely high 2DEG density of 1.8*10 cm at 77K which is about two times that of a regular SH HEMT. Depletion- mode HEMT's have been fabricated using these double heterostructure. The highest transconductance measured for these DH HEMT's with 1 μm gate length at room temperature was 300 mS/mm. This is the highest transconductance value reported to date for depletion-mode HEMT's.

Because of the very high two-dimensional electron concentration and very low resistance achieved in DH HEMT's, these devices can be operated in a wide gate voltage range without any transconductance degradation. DH HEMT's should find applications in both low-noise and medium-power microwave and millimeter-wave devices as well as ultra high speed digital and signal processing IC's.

Modulation doped structure in AlInAs/GaInAs have exhibited higher room temperature mobilities than those of AlGaAs/GaAs of the same electron sheet density. For this reason, modulation doped AlInAs/GaInAs FET's are currently being studied at UCSD by Professors Wieder and Ku to emphasize room temperature performance.

2.3 Heterojunction Bipolar Transistors

With the emergence of MBE, the possibility of fabricating bipolar transistors with a wide bandgap emitter has become feasible. In homojunction npn transistors, the injection of holes from the base into the emitter is minimized by a high emitter to base doping density ration thereby improving the emitter injection efficiency. For high frequency transistors, the base width is minimized to shorten the electron transit time across the base. However, for the low-doped narrow base, the lateral base resistance is very large which severely degrades the maximum frequency of operation. With a wide bandgap emitter (GaAlAs), the injection of hole is negligible due to the barrier of the difference in bandgaps even with a heavily doped, low resistance base. For a 1 μm GaAlAs emitter and 500 Å base-width grown by MBE, f_T values of 100-200 GHz have been calculated.

An important benefit of bipolar transistor is that the threshold voltage is determined by the energy gap (a material parameter) of the base and the emitter and only logarithmically on the doping profile and thus independent of geometrical factors. The standard deviation of the threshold voltage can be as low as several millivolts over the entire wafer. HBT's have the potentials of lower logic swings and high process yields. For digital circuit applications, frequency dividers using HBT's have demonstrated input frequency exceeding 10 GHz and the predicted switching speeds are in the 10 ps range.

For analog applications, HBT's offer an attractive candidate for operations in the 50-100 GHz range. Recently, an inverted A/GaAs/GaAs heterojunction bipolar transistor structure utilizing heterojunction injection and ballistic electron motion in GaAs has been designed and fabricated. This inverted HBT structure has demonstrated microwave performance in the 10-20 GHz frequency range with 2 μm emitter by Zhu, Ku, and Wood.

Performances of the GaA/As/GaAs heterojunction bipolar transistors indicate that parasitics such as base contact resistance are a major limitation to high frequency performance. Ion implanted contacts and tailoring of doped profiles are two methods which can be used to reduce this problem. In addition, HBT's can be fabricated with A/InAs or A/GaInAs emitters and GaInAs bases and collectors can be grown by MBE. The quarternary emitter may be necessary to avoid injecting electrons from the emitter directly into the upper valley of the base. HBT's with wide bandgap emitters will be studied for applications to analog (microwave and millimeter solid state devices) IC's.

The high speed performance offered by HEMT and HBT devices opens a wide area of circuit applications. For the next generation computers, CPU's with a performance of 100 Million Instructions Per Second (MIPS) and a system delay of 100 ps will be possible for VLSI circuits with more than 10K gates. Such performance will place HEMT's HBT's as the most promising device candidate to satisfy CPU and cache memory requirements for the main-frames of future computers. In addition, these devices will also provide new building blocks for the next-generation ultra high speed signal processing and monolithically integrated E/O systems.

3. A LARGE-SIGNAL HEMT MODEL

The high electron mobility transistor has shown it superiority over GaAs MESFET in the application as a low noise amplifier in the microwave frequency range. As in the case of MESFET, with advances in fabrication technology and device structure, the HEMT application will move into the realm of nonlinear circuits rapidly.

The power performance of HEMT's with single-heterojunction and double-heterojunction have been investigated. Mass et al. reported a HEMT mixer to operate at 45 GHz. These promising results indicate that the HEMT will no longer be confined in small-signal application.

For both the small-signal and large-signal applications of GaAs MESFET's, computer aided design proves to be invaluable in the design process, especially in the field of monolithic integrated circuits, where tuning the circuits to get optimal performance is impossible. This underscore the significance of a well-developed device model, on which the accuracy and efficiency of computer aided design and simulation rely. A large-signal HEMT model to serve this purpose is discussed in this section.

Since the HEMT technology is not yet mature in the present time, the understanding of HEMT's behavior under large-signal operation is relatively poor. In this chapter, the development of HEMT large-signal model is analogous to that of GaAs MESFET. This approach is somehow justified by the similarities the HEMT and the GaAs MESFET possess. For example, the generally accepted small-signal equivalent circuits for the HEMT is borrowed from that of the MESFET. As a result, we tried to derive the HEMT large-signal model from the achievements in modeling the GaAs MESFET. Next section will address the general approaches in large-signal modeling with emphasis on GaAs MESFET. These approaches are all equally applicable to the HEMT large-signal model.

3.1 The Modeling Approaches

Since the advent of the GaAs MESFET, many effort have been devoted to develop a computationally efficient model that can simulate the operation of a GaAs MESFET. To achieve this goal requires compromise between the sophistication of solid-state physics and practical demands of electrical engineering. Based on the compromise made on the physical implication and engineering application, the existing GaAs MESFET models in general can be divided into the following four classes:

(1) Two-dimensional numerical models - detailed two-dimensional models based on doping profiles and numerical solutions to the coupled nonlinear semiconduction device equations with appropriate boundary conditions. These models include conventional two-dimensional models, Monte-Carlo particle models, hydrodynamic models , and electron temperature model. The numerical results obtained from these models are very helpful to gain insights into the device operation but long computation time make this approach impractical in the application of circuit analysis and simulation. A two-dimensional simulation with hydrodynamic equations are recently been performed on the MEMT;

(2) Simplified two-dimensional models - Based on the results of two-dimensional simulation of GaAs MESFET, Yamaguchi and Kodera formulated a simplified model for the carrier density under the gate as an implicit function of the internal gate-source and drain-source voltages. The drain current can then be calculated easily. Models following this approach are those proposed by Madjar and Rosenbaum and by Shur and Eastman. Although both models require less computation time than the detailed

two-dimensional model, they are still of limited use in design and analysis of complicated circuits. Besides the MESFET physical parameters used in these models are rarely available to the circuit designer.

(3) Nonlinear circuit models - These models use analytical or empirical equations such as DC current-voltage equation and Schottky diode equation to describe the nonlinear property of the lumped equivalent circuit elements. This kind of models give a more phenomenological than physical picture. However, they provide an easy way to handle device-circuit interaction and hence more suitable for computer aided design and circuit simulation. The works by Tajima and Materka fall in this class.

(4) Black box method - This approach relies on a set of small-signal S-parameter measurements to characterize the nonlinear behavior of an actual device. The results are used to formulate an equivalent circuit by using polynomial expansion to approximate the bias-dependency of the circuit elements. This si exemplified in the works of Willing and Rauscher. The major drawback of such an approach is numerous S-parameter measurements must be done to characterize the device. Furthermore, the working conditions for GaAs MESFET under small-signal measurement and large-signal operation may be different, which renders the validity of this quasi-static approach questionable.

After considering all the approaches described above, we developed a large-signal model which is a combination of the models in class 3 and class 4. First, the compact HEMT I-V model derived in the previous chapter is used to model the principal nonlinear elements of the GaAs MESFET, i.e., transconductance and output conductance. The complete large-signal model is subsequently constructed from the small-signal equivalent circuit by including other nonlinearities necessary to describe the HEMT behavior under large-signal operation. The nonlinear elements in this model is then characterized by the results from small-signal S-parameter measurements as class 4 models.

3.2 The Large-Signal Model

Under large-signal operation, element values of the HEMT equivalent circuits shown in Fig. 3.1 vary with time and become dependent on the terminal voltages. A large-signal model can be derived by considering the main nonlinear elements of the equivalent circuit. Referring to Fig. 3.2, the main nonlinear behavior of a HEMT is assumed in our model to result from the following nonlinear elements:

(1) the drain current source, I_d, controlled by the internal voltages, V_g and V_d. This voltage-controlled source accounts for the nonlinearities of g_m and R_{ds} in the small-signal equivalent circuit;

(2) the gate-to-source capacitance, C_{gs};

(3) the gate-to-drain capacitance, C_{dg};

(4) the current source, I_f, which represents the current flow through the Schottky gate. The effect of this current source will become important only when the gate is forward-biased.

(5) the current source, I_r, which represents the gate-drain breakdown phenomenon. In the case of GaAs MESFET's, I_f and I_r are the main power-limiting factors of a power amplifier.

In this large-signal model, the drain current source, I_d, is expressed by the current-voltage equations derived in [1].

Theoretically, C_{gs} and C_{dg} can be derived from the charge control model presented in [1]. From the experimental results, these two capacitances behaves quite similar to those of a MESFET, due to the fact that a lot of excessive charge in addition to the two-dimensional electrons are modulated by the terminal voltages. Hence a much simpler approach without losing reality is using empirical Schottky diode equations to relate C_{gs} and C_{dg} to the terminal voltages. We model these two nonlinear capacitances by

$$C_{gs} = \frac{C_{gso}}{(1 - \frac{V_g}{V_{bi}})^n} \tag{3.1}$$

and

$$C_{dg} = \frac{C_{dgo}}{(1 - \frac{V_{dg}}{V_{bi}})^m} \tag{3.2}$$

where C_{gso}, n, C_{gdo}, and m are modeling parameters adjusted to fit the measured values. V_{bi} is the build-in voltage for the Schottky gate. In the case of a MESFET, the values of m and n are close to 0.5.

The gate-forward conducting current, I_f is given by a simple diode equations as

$$I_f = I_{fo}(e^{\alpha_f V_g} - 1) \tag{3.3}$$

with I_{fo} and α_f as modeling parameters. The gate-drain current, I_r is represented by

$$I_r = I_{ro}(e^{\alpha_r V_{dg}} - 1) \tag{3.4}$$

where I_{ro} and α_r are modeling parameters. Note the models for these two currents are similar to those of a MESFET [39], [45]. More experimental results are needed to support the diode model when applying the gate-drain breakdown effect in the HEMT.

Only at extreme conditions of positive gate voltages exceeding the Schottky gate build-in voltage do the nonlinear forward conducting gate current starts to flow. Similarly, the drain-gate breakdown current conducts at large drain voltage and low gate voltage. The effects of the two currents are to limit the current delivered to the load and to clip the input voltage waveforms. Thus these currents will affect the gain compression at large-signal level and contribute to the harmonic generation of the current and voltage waveforms. In HEMT's application for moderate power level and without the involvement of these two current sources, such as mixers, these currents can be neglected and a minimum set of nonlinear elements: (C_{gs}, g_m, R_{ds}) is generally sufficient. For simplicity of computer simulation, the nonlinearity of C_{dg} is also neglected. This will not cause significant error, due to its relative small value and function as a feedback element, compared to C_{gs} which determines the input impedance. The assumption that C_{dg} is constant is especially true when current is saturation. The simplified large-signal model is shown in Fig. 3.3.

3.3 Practical Examples

The two HEMT's, TRW #2241 and GE #5415, served as modeling examples of DC characteristics [1] are again used for the purpose of large-signal modeling. In this section bias-dependent S-parameter set and DC characteristics are used to build the simplified large-signal

model.

3.3.1 Large-signal model of TRW #2241

The large-signal modeling of this TRW HEMT started from extracting the small-signal equivalent circuits from the measured S-parameters at two bias points: $V_{GS} = 0.3 V_{DS} = 3.0\ V$. Since only C_{gs}, G_m, elements, other equivalent circuit elements are adjusted to have identical values at different bias. The element values of the small-signal equivalent circuits at the two bias points are shown in Table 3.1. Also indicated are the r.m.s. errors of the fitting between the measured and modeled S-parameters.

Bias	$V_{GS} = 0.3\ V$ $V_{DS} = 3.0\ V$	$V_{GS} = 0.5\ V$ $V_{DS} = 3.0\ V$
$g_m(mS)$	19.73	25.91
$C_{gs}(pF)$	0.0867	0.101
$R_i\ (\Omega)$	2.1	2.1
$C_{ds}(pF)$	0.05	0.05
$R_{ds}\ (\Omega)$	687.8	601.2
$C_{dg}(pF)$	0.008	0.008
$L_s(nH)$	0.01	0.01
$R_s\ (\Omega)$	1.1	1.1
$R_g\ (\Omega)$	8.0	8.0
$L_g(nH)$	0.035	0.035
$R_d\ (\Omega)$	7.8	7.8
$L_d(nH)$	0.025	0.025
τ (ps)	1.6	1.6
error(%)	5.5	4.6

Table 3.1. The element values of small-signal equivalent circuit for TRW #2241 HEMT at two different bias points

The modeling parameters, C_{gso} and m, in the nonlinear C_{gs} model are determined by a simple optimization program to fit the equation to the Cgs's in the bias dependent small-signal equivalent circuits. We find for $C_{gso} = 0.075$ pF and $m = 0.349$, the fitting is perfect, therefore

$$Cgs = \frac{.075}{(1 - \frac{V_g}{.85})^{.349}}$$

Note that V_g is the internal gate voltage. The voltage drops across the parasitic source and drain resistance have to be taken into account for modeling the nonlinear capacitance. The internal gate and drain voltages is automatically calculated when the optimization program is invoked to fit the DC characteristics.

The modeled and measured DC characteristics are shown in [1]. The modeling procedure and modeling parameters has been discussed in the previous chapter. The g_m's and R_{ds}'s calculated from the modeled DC characteristics are compared with those obtained from S-parameters in Table 3.2.

	g_m (mS)		R_{ds} (Ω)		
Bias	DC char.	S-para	DC char.	S-para.	$//R_{off}$
$V_{GS} = 0.3\ V$	19.4	19.7	880	688	650
$V_{GS} = 0.5\ V$	26.3	25.9	863	601	640

Table 3.2. Comparison of transconductance and output conductance from DC characteristics and S-parameters of TRW #2241 HEMT

We observe that the output resistance calculated from modeled DC characteristics are higher than those from S-parameters, while the transconductances are about the same. The discrepancy in the output resistance is thought mainly due to the slow dynamics of electron emission capture by the traps, which is unable to catch up with the device operation at microwave frequency. The frequency dependency of the output resistance of a MESFET has been reported in [ ]. Therefore, an offset resistance, R_{off}, equal to 2483 Ω is added in shunt to the current source to adjust the fitting between the R_{ds} obtained from DC characteristics and S-parameters. The adjusted results are also shown in Table 3.2.

The large-signal model of TRW #2241 HEMT is shown in Fig. 3.4 (R_{off} not included). The S-parameters calculated from the large-signal model is compared with the measured S-parameters in Fig. 3.5. (a) (b). The r.m.s. error of the modeled and measured S-parameters are 6.8% and 6.4% for the bias at $V_{GS} = 0.3\ V$ and $V_{GS} = 0.5\ V$, respectively. These results are comparable to those obtained from using small-signal equivalent circuit to model the S-parameter. The advantage of this model is the S-parameters at any bias points can be directly calculated, while small-signal equivalent circuit is useful for only a fixed bias point.

3.3.2 Large-signal model of GE #5415 HEMT

The modeling procedure of this GE #5415 HEMT is the same as that of TRW #2241. From the measured S-parameters at two bias points, the small-signal equivalent circuits are constructed, whose element values are summarized in Table 3.3.

Bias	$V_{GS} = -0.2\ V$ $V_{DS} = 2.0\ V$	$V_{GS} = -0.5\ V$ $V_{DS} = 2.0\ V$
$g_m(mS)$	29.26	39.14
$C_{gs}(pF)$	0.149	0.128
$R_i\ (\Omega)$	10.8	10.8
$C_{ds}(pF)$	0.061	0.061
$R_{ds}\ (\Omega)$	293	233
$C_{dg}(pF)$	0.023	0.023
$L_s(nH)$	0.001	0.001
$R_s\ (\Omega)$	3.8	3.8
$R_g\ (\Omega)$	3.2	3.2
$L_g(nH)$	0.32	0.32
$R_d\ (\Omega)$	4.6	4.6
$L_d(nH)$	0.28	0.28
τ (ps)	1.3	1.3
error(%)	5.7	5.9

Table 3.3. The element values of small-signal equivalent circuits for GE #5415 HEMT at two different bias points

The DC characteristics of this device has already been modeled and the result is shown in [1]. Table 3.4 compares the transconductance and output resistance obtained from DC characteristics and S-parameters.

	g_m (mS)			
Bias	DC char.	S-para	DC char.	S-para.
$V_{GS} = -0.2\ V$	30.4	29.3	213	239
$V_{GS} = -0.5\ V$	42.7	39.1	254	233

Table 3.4. Comparison of transconductance and output conductance from DC characteristics and S-parameters for GE #5415 HEMT

No R_{ds} adjustment is necessary since the agreement between R_{ds} from DC characteristics and that from S-parameters is reasonable good. The nonlinear gate capacitance is modeled as

$$C_{gs} = \frac{.178}{(1 - \frac{V_g}{0.8})^{.67}}\ pF\ .$$

The large-signal model of this device is depicted in Fig. 3.6 with the comparison of the measured S-parameters and those calculated from this model shown in Fig. 3.7 (a) (b). The r.m.s. errors for the matching of the S-parameters are 6.8% and 7.9% for gate bias at $V_{GS} = -0.2\ V$ and $V_{GS} = -0.5\ V$. The results are also comparable to that of the small-signal model.

Note that the modeling parameter, m, for the nonlinear gate capacitance in the large-signal model of GE device is higher than in that of TRW device. This stronger variation of C_{gs} vs. V_g is due to the parasitic conduction in AlGaAs. When the AlGaAs layer is not fully depleted, the concentration of two-dimensional electron gas channel is no longer modulated by the gate voltage. Instead, the gate voltage modulate the charges in AlGaAs layer which acts just like a MESFET. One bias point, $V_{GS} = -0.2\ V$ and $V_{DS} = 2.0\ V$, for the GE HEMT fall in the parasitic conduction region and a higher value of m is therefore needed. For the TRW HEMT, no parasitic conduction is shown in the DC characteristics. The C_{gs} varies more lowly with the V_g as predicted from the analytical theory.

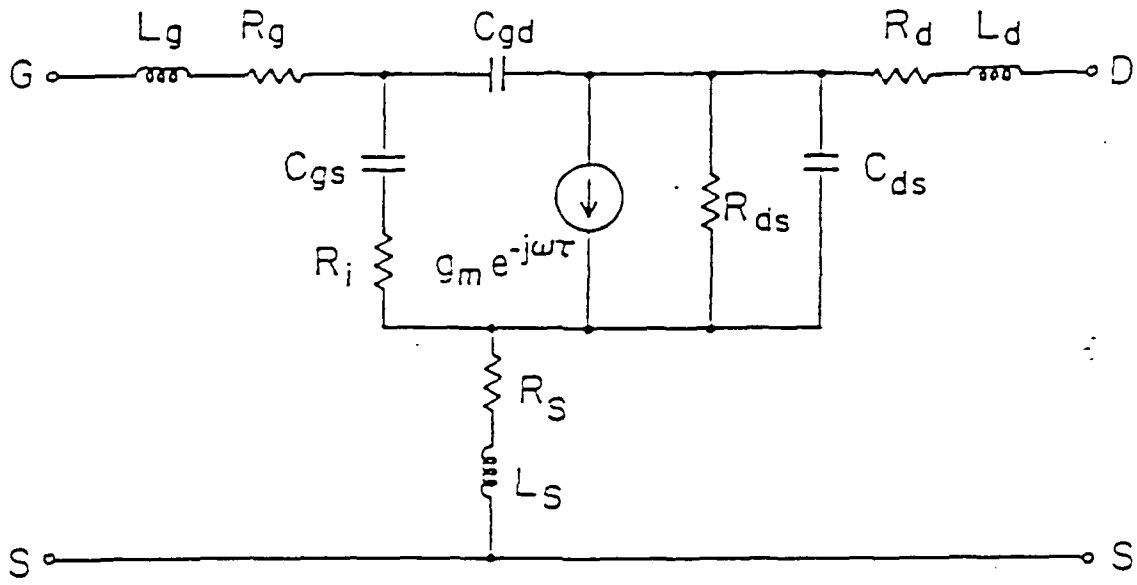

Figure 3.1. Small-signal equivalent circuit of the HEMT

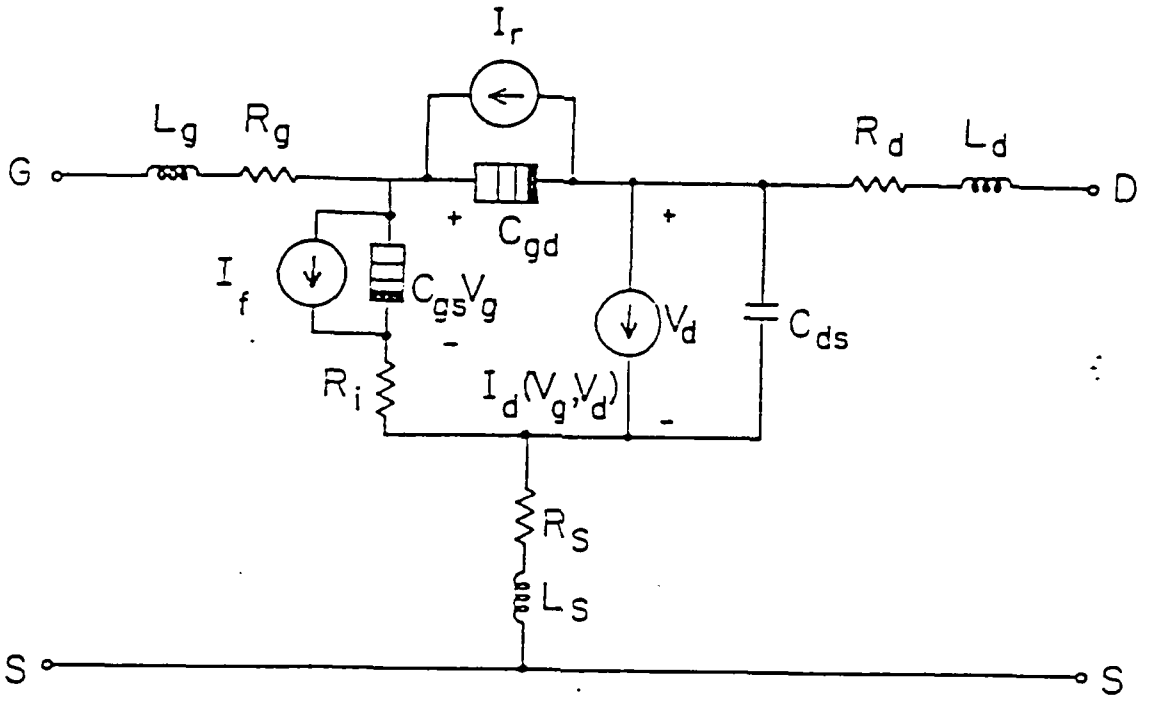

Figure 3.2. Large-signal model of the HEMT

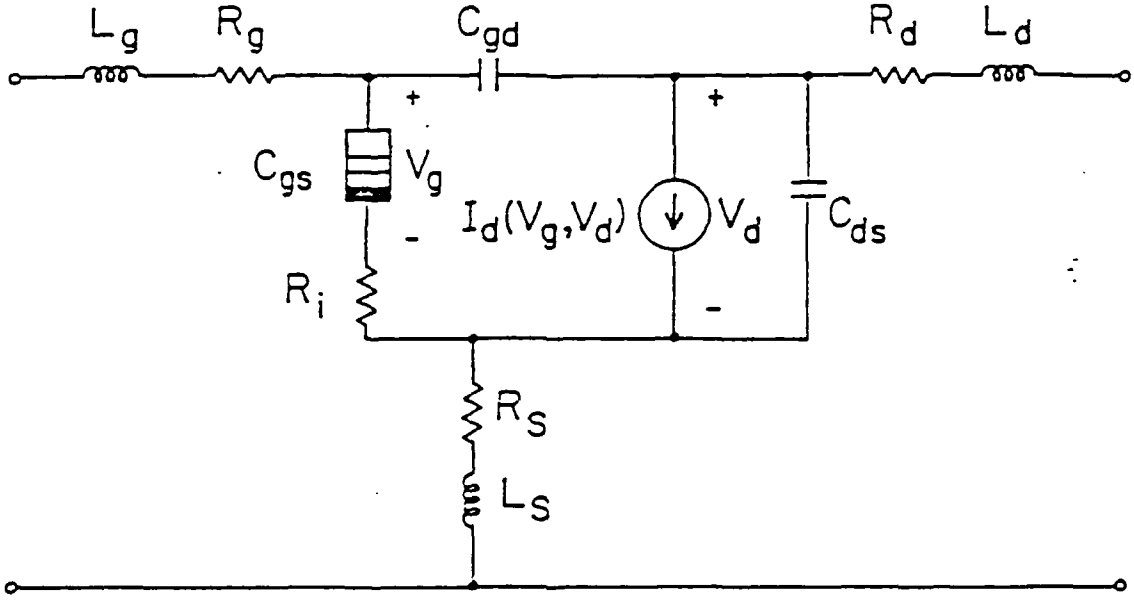

Figure 3.3. Simplified large-signal model of the HEMT

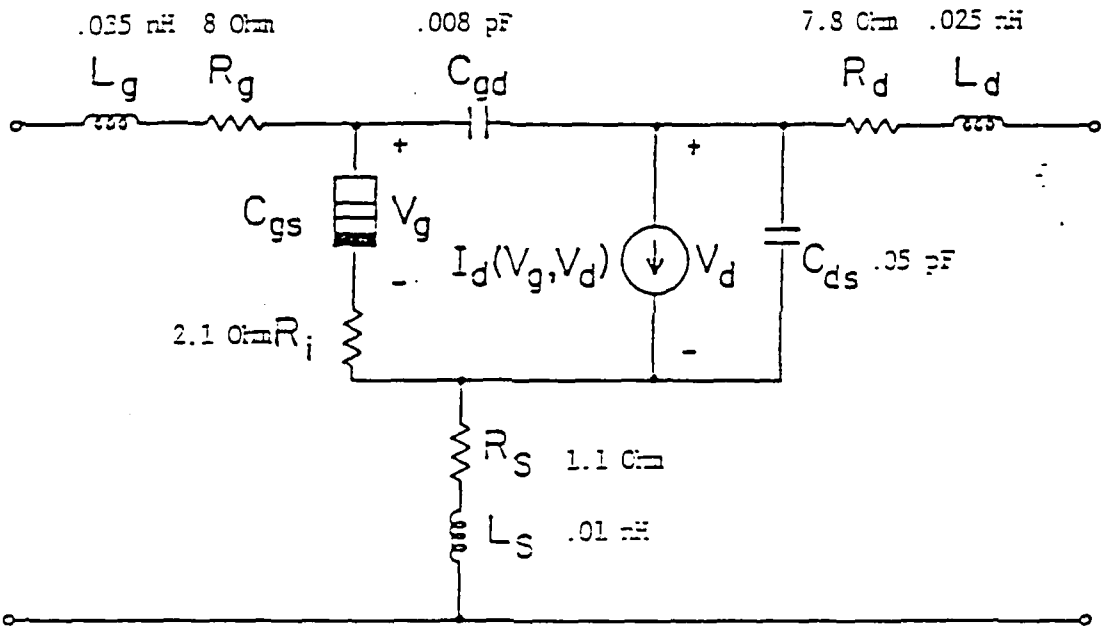

Figure 3.4. Simplified large-signal model of TRW #2241 HEMT

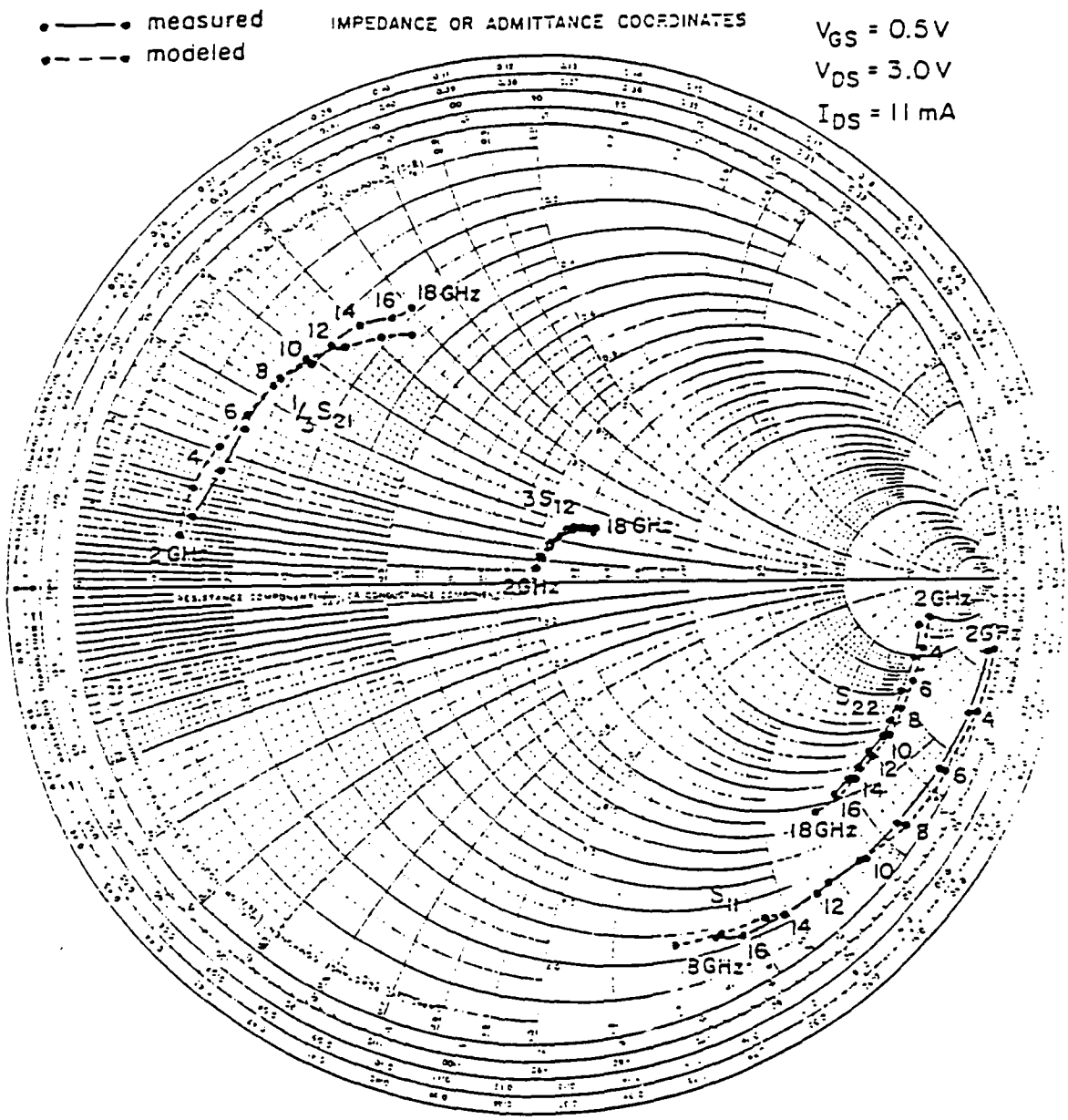

Figure 3.5(a). Measured and calculated S-parameters at different bias

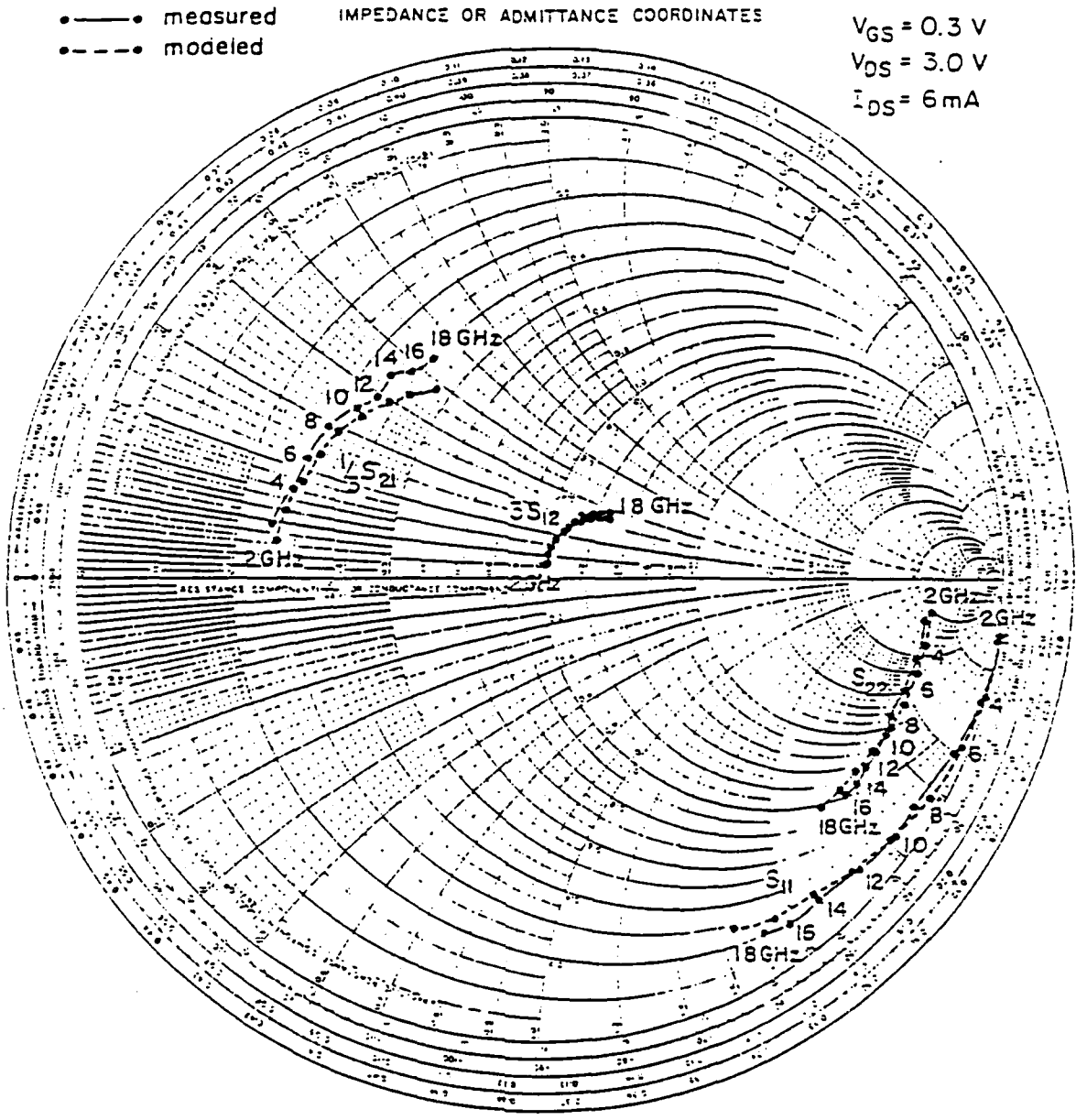

Figure 3.5(b). Measured and calculated S-parameters at different bias

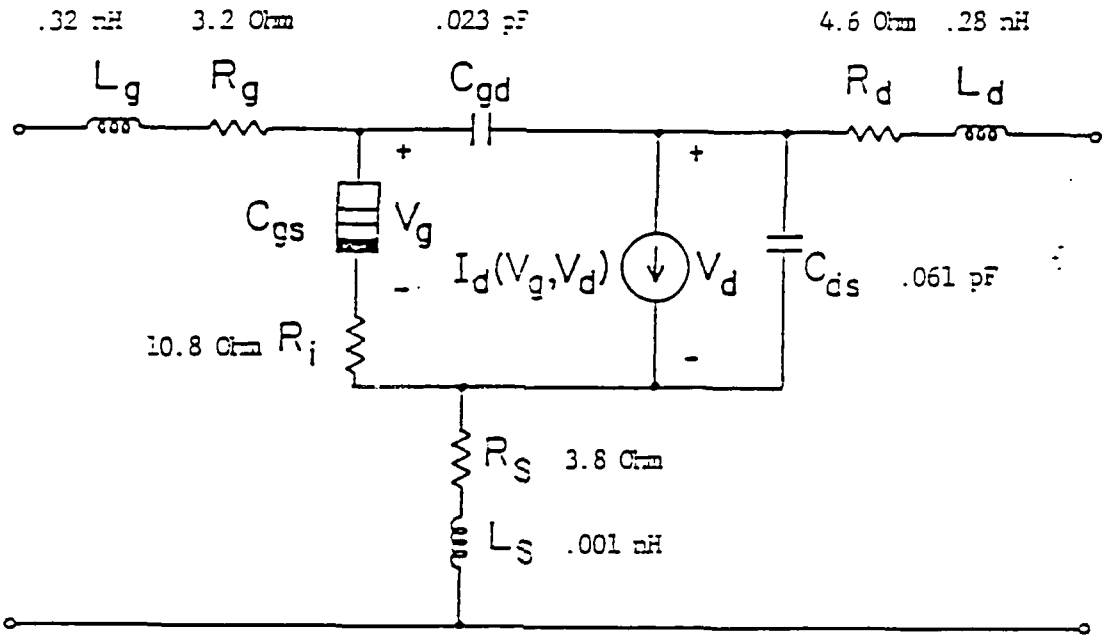

Figure 3.6. Simplified large-signal model of GE #5415 HEMT

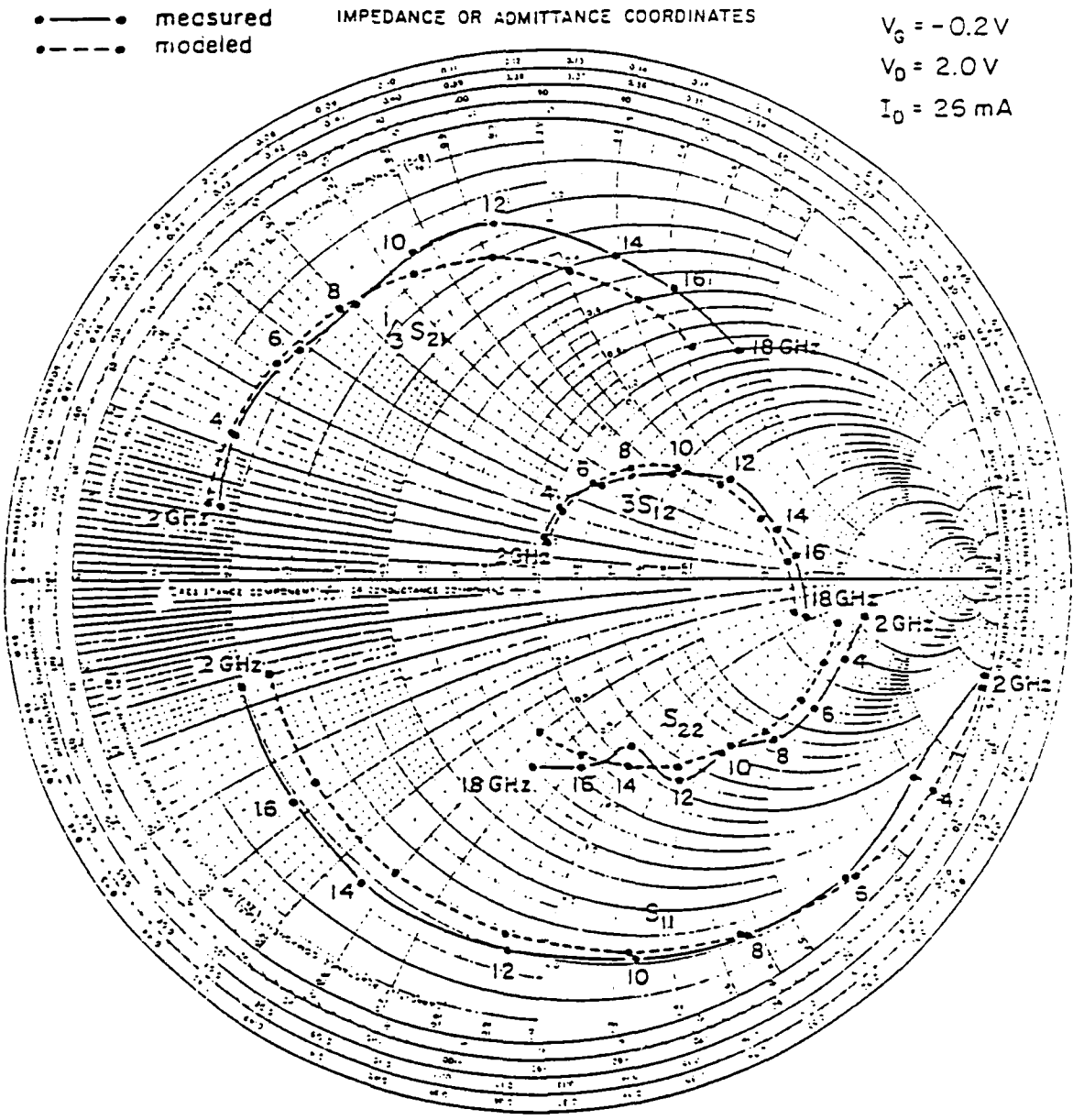

Figure 3.7(a). Measured and calculated S-parameters at different bias

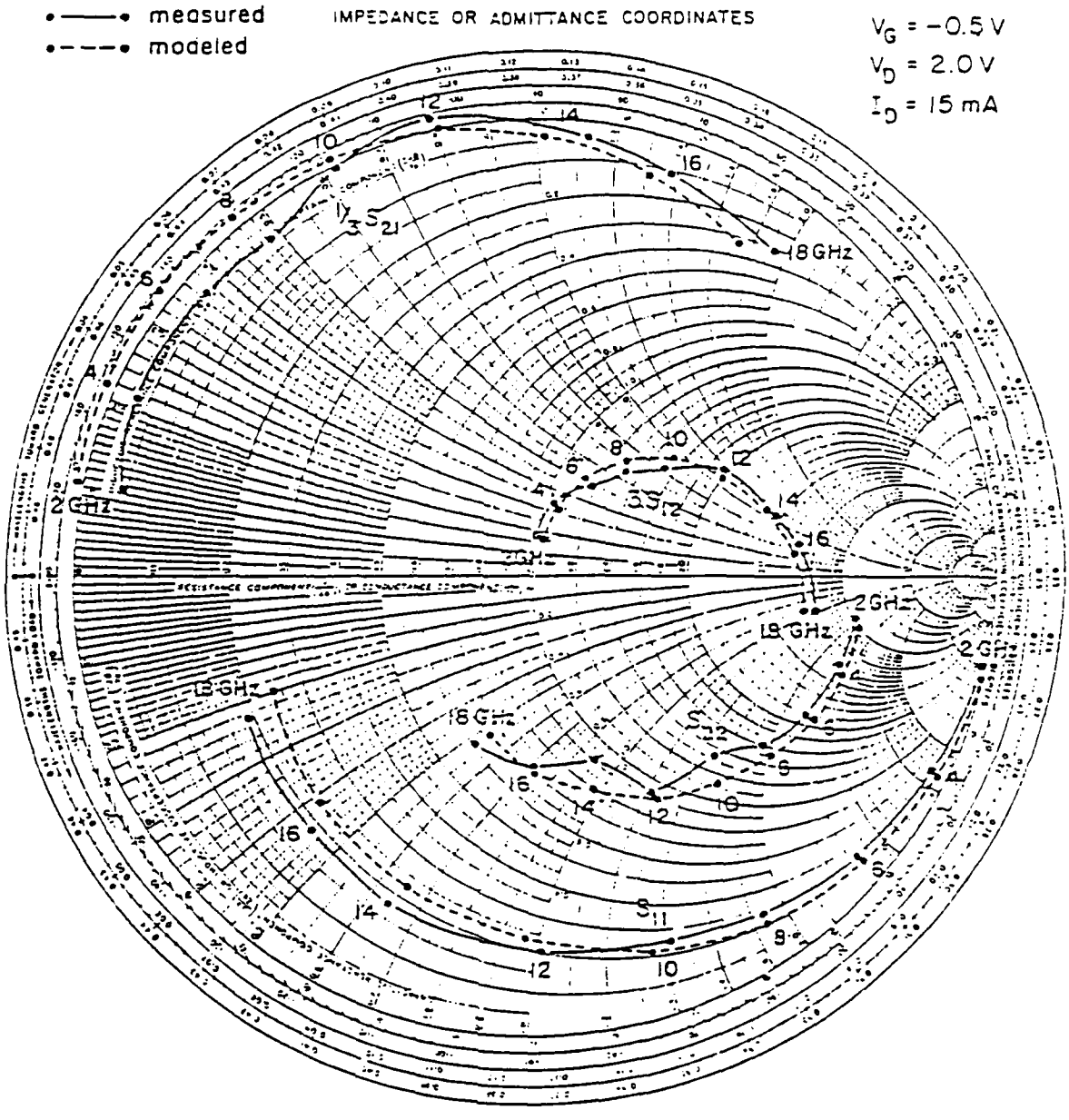

Figure 3.7(b). Measured and calculated S-parameters at different bias

4. HEMT MIXERS

4.1 Introduction

Frequency conversion for signals carrying information is a common practice in microwave communication. The frequency conversion or mixing is obtainable through the interaction of the radio frequency signal (SI), generally after the amplification by the RF low-noise amplifier, with the signal coming after the amplification by the RF low-noise amplifier, with the signal coming from a local oscillator (LO) in a nonlinear circuit, which is then called a mixer. The desired intermediate frequency, usually the difference between the SI and LO frequencies, is selected from the resulting mixing products. Accordingly, the RF amplifier, the local oscillator, and the mixer constitute the basic building blocks of a receiver front.

A figure of merit for frequency conversion is the conversion gain, which is defined as the ratio of IF power delivered to the load to the RF power available from the generator. In a microwave receiver the mixer is usually followed by an IF amplifier. High conversion gain and low noise figure for a mixer is important because the noise figure of the receiver will essentially be that of the mixer with very little contribution from the IF amplifier noise.

Schottky barrier diodes which utilize the nonlinearity of the metal-semiconductor current-voltage characteristics have been in wide use as mixers. Along with the rapid improvement of the GaAs MESFET technology, the application of the MESFET as a microwave mixer has attracted considerable attention, due to its advantages over the diode mixer. Among the advantages is the possibility to achieve both high conversion gain and low noise figure, as well as the easy isolation between various frequency components existing in a mixer.

There are two different types of MESFET mixer circuits, according to the device nonlinearity being used. The gate mixer uses the nonlinear Id-Vg characteristics, with LO signal injected into the gate circuit, while in a drain mixer, the LO signal is fed into the drain circuit to use the nonlinear Id-Vd characteristics. Most of the studies for the MESFET mixers are devoted to the gate mixer. Comparison made by Bura et al. shows that the noise figure of the drain mixer is lower than that of the gate mixer, although the conversion gains are about the same.

Dual-gate MESFET mixers have also been the subject of considerable investigations due to the easy isolation of LO and RF signals by injecting the two signals into the different gate

terminals, which not only greatly reduces the complexity of the associated external circuit but also increases the flexibility of the circuit structure. With different bias conditions and circuit structures, many modes of operation are possible, such as self-oscillating mixer and image rejection mixers. This makes the dual-gate MESFET mixers particularly attractive for monolithic integrated circuits.

Although the noise figure of a MESFET mixer is comparable to a diode mixer, the MESFET functions as a mixer has only been demonstrated up to the X-band, compared to the diode mixer's operation which goes far into the millimeter-wave region.

For its extremely high gain and low noise figure, the HEMT has been proved to be the device of choice for low noise amplification in millimeter-wave range. The HEMT used as a millimeter wave mixer will have all the advantages that the MESFET mixer has over the diode mixer, while high conversion gain and low noise figure are possible in the frequency range where the MESFET mixer is inadequate to operate. Recently, Maas of TRW has reported a HEMT mixer reporting at 45 GHz. With IF frequency equal to 3 GHz, the HEMT mixer shows a 1.5 maximum conversion gain and 8.1 dB noise figure with an associated conversion gain of 1 dB. These results demonstrate that HEMT mixers can be used in the millimeter-wave receiver with high conversion gain and noise figure that is comparable to good-quality diode mixers.

This section presents the computer aided design and analysis of the HEMT mixer, using the large-signal model and the time domain nonlinear program, *CADNON*. The transconductance compression effects on the performance of the HEMT as a mixer are also studied.

4.2 The Design Method

Owing to the nonlinear nature of the problem, to design a mixer with the maximum conversion gain available from the device, a systematic computer aided design method seems to be the only choice. A nonlinear time domain program, *CADNON*, suitable for microwave GaAs MESFET circuit simulation has been developed. A brief introduction of the program is given in Appendix A. Modifications of this program to accept the large-signal HEMT model described in the previous chapters has been done.

Based on this program, a systematic method to design a mixer using HEMTs or MESFETs is present in this section. Note that with some modification, the design method can be applied to find the optimum source and load conditions for maximum output power and consequently design the matching networks of power amplifiers and embedding networks for oscillators.

The computer aided design of a HEMT mixer proceeds as follows:

(1) A large capacitor is added in shunt to the device to provide the low impedance path for the LO and SI frequencies. If the circuit is to be built by distributive elements, a quarter-wave length open stub can also serve this purpose. We call this combination a basic mixer (Fig. 4.1(a)).

(2) At desired operating frequencies, f_{SI} and f_{LO}, LO signal with different power levels are applied to find the maximum output power at the IF frequency and the corresponding input impedance at SI frequency. The circuit configuration for *CADNON* simulation at this step is shown in Fig. 4.1(a).

(3) Design an input matching network to provide impedance matching between the input impedance of the basic mixer and the source impedance at SI frequency. Since this is just a single-frequency matching problem, design method using Smith chart or any computer aided synthesis program such as *CADSYN*^{TM} will suffice.

(4) The output impedance at IF is found for the cascade of the input matching network and the basic mixer. The LO power is maintained at the same level that provides maximum IF output power (Fig. 4.1(b)).

(5) Design the output matching network to provide the impedance matching at IF frequency. An initial design of the mixer is complete by cascading the input matching

network, the basic mixer, and the output matching network.

(6) Repeat step 2, except that now the basic mixer is replaced by the initial design of the mixer. Referring to Fig. 4.1(c), the Γ_{in} and Γ_{in} are found at maximum IF output power for various LO power level. Generally, the LO power corresponding to the maximum IF output power will be slightly lower than that found in step 2, due to the effect of input matching which actually has more LO power delivered into the device. From Γ_{in}, we can determine the input mismatch at SI frequency for this particular configuration, i.e., input and output matching and LO power level. If considerable mismatch is found, design a new matching network according to Γ_{in}.

(7) With the newly designed input matching network, if any, the output IF impedance is determined as in step 4. This step is illustrated in Fig. 4.1(d). If the Γ_{out} shows deterioration of the output matching, a new output matching network has to be designed according to Γ_{out}.

(8) Repeat steps 6 and 7 until good matching at the input and output ports of the mixer is obtained at the maximum IF output power. Generally speaking, one or two iterations after the initial design is sufficient.

In the above iterative procedures, a maximum mixer conversion gain available from the device is ensured due to the simultaneous adjustments of the matching networks for impedance matching and for optimum source and load conditions for the device to generate maximum output power at the IF frequency.

4.3 Design and Simulation of the HEMT Mixer

Following the design procedure described in the previous section step by step, the designs of HEMT mixers operating at 10, 20, 40 GHz have been carried out. The device used is GE #5415 HEMT whose DC characteristics and large-signal model are shown in Fig. 2.14 and Fig. 3.6, respectively. The bond wire inductances, L_g and L_d are deleted from the large-signal model in these mixer designs. The SI power level is set at -30 dBm and the bias is chosen at V_{GS} = -0.8 V and V_{DS} = 2.0 V. Figure 4.2 shows the circuit diagram of the mixers with the element values of the matching networks summarized in Table 4.1 for each operating frequency. The IF remains 2 GHz in all the cases.

For the mixer design to operate at f_{SI} =u 10 GHz and f_{LO} = 8 GHz, the optimal LO power is 2 dBm for a maximum conversion gain as high as 9 dB (Fig. 4.3(a)). This result compared favorably with the 6 dB maximum conversion gain generally obtained at X-band by GaAs MESFET mixers. The input VSWR at 10 GHz and output VSWR at 2 GHz are also calculated and shown in Fig. 4.3(b). The low VSWR's ensure that the mixer is operating in optimal conditions for conversion gain.

The performance of the mixer operating at f_{SI} = 20 GHz and F_{LO} = 18 GHz are demonstrated in Fig. 4.4(a). A maximum conversion gain of 3.6 dB is achieved at a LO power of -0.46 dBm. The input and output VSWR's at signal and intermediate frequencies in Fig. 4.4(b) again shows that an optimal design is achieved. To the author's knowledge, there is no published report on GaAs MESFET mixers designed to operate around this frequency range.

To investigate the feasibility of millimeter-wave mixers using the HEMTs, a HEMT mixer is designed and simulated at 40 GHa. Instead of conversion gain, the mixer shows a minimum conversion loss of 2 dB at LO power equal to 2 dBm (Fig. 4.5(a)). The VSWR's in Fig. 4.5(b) implies we can't obtain more conversion gain from the GE #5415 HEMT as a mixer operating at f_{SI} = 40 GHz and f_{LO} = 38 GHz. The maximum conversion gain at these three operating frequencies along with the average drain current and LO power are summarized in Table 4.2.

We observe in Table 4.2 that the maximum conversion gain shows a slope around 5.5 dB/oct, which is just close to the ideal maximum available gain slope of the HEMT in small-signal operation, i.e., 6 dB/oct. Considering the nonlinear effect and frequency conversion involved in a mixer, this coincidence is surprising and will be further investigated in Sec. 4.5. The performance of the HEMT mixers designed to operate at 10, 20, and 40 GHz. The frequency characteristics of the mixer operating at 20 GHz is shown in Fig. 4.6. The 3 dB bandwidth is about 4 GHz with the LO power maintained at -0.46 dBm, the optimal value when the HEMT is biased at V_{GS} = -0.8 V and V_{DS} = 2.0 V. Note that the input matching is only done at 20 GHz while the output matching is at 2 GHz.

Conversion gain vs. gate biasing voltage is also studied and shown in Fig. 4.7. The conversion gain shows a dip at V_{GS} = -0.4 V, which has never been observed in a MESFET mixer. The anomalous phenomenon is found due to the effect of transconductance compression.

4.4 Effects of Transconductance Compression on Mixer Performance

A distinct feature of the HEMT as compared to the GaAs MESFET is the strong transconductance compression frequently observed in normal bias range, while the latter occasionally shows this effect slightly when the gate voltage is close or exceeding the zero bias. In GaAs MESFET, the effect is thought to be due to the surface depletion or the velocity ivershoot in a short-channel device.

Fig. 4.8 depicts the calculated g_m vs. V_{GS} of the GE #5415 HEMT. Distinctive transconductance compression is observed in this figure when the gate biasing voltage exceeds -0.5 V. Owing to the near symmetrical dependency of g_m on V_{GS}, when the gate is biased at -0.4 V, the odd components of the Fourier series expansion of the g_m as a periodic function with a period equal to the LO's will almost vanish. But how are the Fourier components related to the conversion gain?

Qualitatively, the mixer operation can be conceptually visualized as follows: when a strong sinusoidal LO voltage is impressed between the gate and source, the principal nonlinear elements, C_{gs}, and g_m, and R_{ds}, will become a periodic function of time with the same period as the LO. The nonlinear elements can then be expanded as a Fourier series with fundamental frequency equal to the LO frequency. Among these Fourier components, g_{g_1}, which is the fundamental frequency component of g_m, is the most significant factor to determine the conversion gain. Through g_{m_1} the signal frequency component of the internal gate voltage is down converted to drain current at intermediate frequency. This is the main frequency conversion path from signal to intermediate frequency in a gate mixer, in which the g_m nonlinearity is utilized to a greater extent than any other nonlinear element. We will use perturbation analysis to study the frequency conversion in a HEMT mixer in Sec. 4.5.

To prove our point that the dip in the conversion gain characteristics is due to the transconductance compression, the same GE #5415 HEMT is used in the mixer circuit except the parasitic conduction is removed from the I-V model (Fig. 4.9). This can be easily done in our I-V model by setting V_c much larger than the gate voltage which may occur during the mixer operation. With this modified HEMT and all the operating conditions remaining unchanged, the conversion gain vs. gate bias is calculated and shown in Fig. 4.10. We observe that the dip in the

original conversion gain characteristics disappears and the conversion gain increases by 2 dB.

The conclusion is that transconductance compression will degrade the performance of the HEMT mixer. The gate bias has to be properly chosen for the HEMT which shows transconductance compression to avoid the vanishing point of the conversion gain. Our simulation indicates that higher conversion gain can be obtained by biasing the HEMT near pinch-off condition (Fig. 4.7).

To further investigate the effect of the effect of the transconductance compression on the conversion gain, we replace the original GE #5415 HEMT by the modified HEMT in the mixer operating at 40 GHz. Fig. 4.11 shows the conversion gain vs. LO power. An increase of the maximum conversion gain from -2 dB to 0.75 dB is observed. This suggests a mixer for millimeter-wave application, which provides conversion gain instead of conversion loss, is possible by using properly designed HEMT's such as those showing no transconductance compression in the DC characteristics. In addition, we find the rugged appearance of the conversion gain curve in Fig. 4.11 can be removed by including only the first two Fourier components of the nonlinear elements in the calculation of the conversion gain. The comparison made in Fig. 4.12 indicated the rugged appearance of the conversion gain curve actually comes from the higher order Fourier components. The calculation is carried out by the perturbation analysis.

4.5 Perturbation Analysis

Perturbation method for mixer analysis considers the RF signal as a small perturbation to the mixer steady state established by the large-signal LO. As mentioned in the previous section, when a mixer circuit is driven by a strong LO signal, the nonlinear elements in the mixer can be considered as a time-vary function with a period equal to the LO period. Therefore, the nonlinear elements as a function of time can be represented by a Fourier series, i.e., into a mixer circuit

$$C_{gs}(t) = C_{gs_0} + \sum_{n=1}^{\infty} C_{gs_n} \cos(n\,\omega_{LO} t + \phi_{C_n}) \tag{4.1}$$

$$g_m(t) = g_{m_0} + \sum_{n=1}^{\infty} g_{m_n} \cos(n\,\omega_{LO} t + \phi_{g_n}) \tag{4.2}$$

$$G_{ds}(t) = G_{ds_0} + \sum_{n=1}^{\infty} G_{ds_n} \cos(n\,\omega_{LO} t + \phi_{G_n}) \tag{4.3}$$

where C_{gs} has its usual meaning and R_{ds} are defined as

$$g_m = \frac{\partial I_d(V_g, V_d)}{\partial V_g} \tag{4.5}$$

$$G_{ds} = \frac{\partial I_d(V_g, V_d)}{\partial V_d}. \tag{4.6}$$

when a low-level radio frequency signal is applied to this mixer circuit, frequency mixing of the LO and SI frequency will generate infinite frequency components. Among these frequency mixing products, only frequencies generated by mixing with fundamental and the first harmonic of the LO frequency are considered non-negligible. Assuming $f_{SI} > f_{LO}$, the significant frequencies in a mixer are the intermediate frequency, f_{IF}, and the image frequency, f_{IM}, which are defined as

$$f_{IF} = f_{SI} - f_{LO} \tag{4.7}$$

$$f_{IM} = 2f_{LO} - f_{SI}. \tag{4.8}$$

The terminal voltages and currents of the mixer at these frequencies can be related to each other by a conversion matrix whose entries consist of the linear elements in the mixer circuit as well as g_{m0}, g_{m1}, C_{gs0}, C_{gs1}, G_{ds0}, *and* G_{ds1}. This conversion matrix method has been frequently applied to the mixer analysis and after some simplification the conversion gain can be directly calculated. To simplify the conversion matrix, certain approximations have to be made, such as a unilateral model for the device; only g_m nonlinearity is considered; only g_m and R_{ds} nonlinearities are considered. However, the results suggest the feedback capacitance in the device has drastic effect on the conversion gain and thus cannot be neglected. It is apparent that the perturbation method and conversion matrix can be managed much better by a computer program.

Perturbation analysis has been performed with *CADNON* on the HEMT mixer. The results are summarized in Table 4.3. The LO power are chosen at those corresponding to maximum conversion gain at each operating frequency (see Table 4.2).

Table 4.1
The element values of the mixer matching networks

Freq.	C_1(pF)	C_2(pF)	L_1(nH)	L_2(nH)	L_3(nH)
10	0.08	2.2	1.23	1.89	0.91
20	0.08	2.2	0.33	1.84	0.96
40	0.1	2.2	0.1	1.99	0.87

Table 4.2
The performance of the HEMT mixers designed to operate at 10, 20, and 40 GHz

$f_{SI}/f_{LO}/f_{IF}$ (GHz)	G_{con} (dB)	I_d (mA)	P_{LO} (dBm)
10/8/22	9.07	9.4	2
20/18/2	3.69	10.1	-0.46
40/38/2	-2.04	8.9	2

Table 4.3
The first three Fourier components of the nonlinear elements and the conversion gains

$f_{SI}/f_{LO}/f_{IF}$ (GHz)	10/8/2	20/18/2	/40/38/2
Cgs_0 (pF)	.12	.119	.117
Cgs_1 (pF)	.0304	.027	.0158
Cgs_2 (pF)	.00293	.00235	.00791
gm_0 (mS)	20.8	21.7	25.7
gm_1 (mS)	20.4	21.3	23.0
gm_2 (mS)	8.52	8.08	6.18
Gds_0 (mS)	2.50	2.50	2.58
Gds_1 (mS)	2.70	2.62	2.02
Gds_2 (mS)	.354	.396	.654
G_{con_1} (dB)	9.07	3.69	-2.04
G_{con_2} (dB)	8.79	3.7	-2.05
G_{con_3} (dB)	10.1	4.6	-0.78

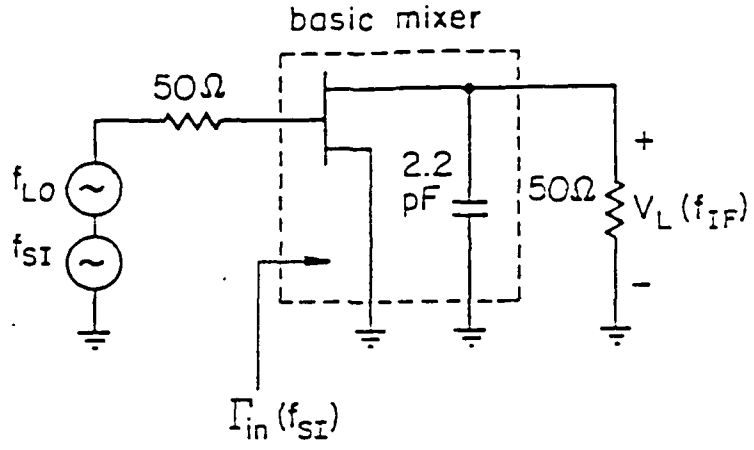

(a)

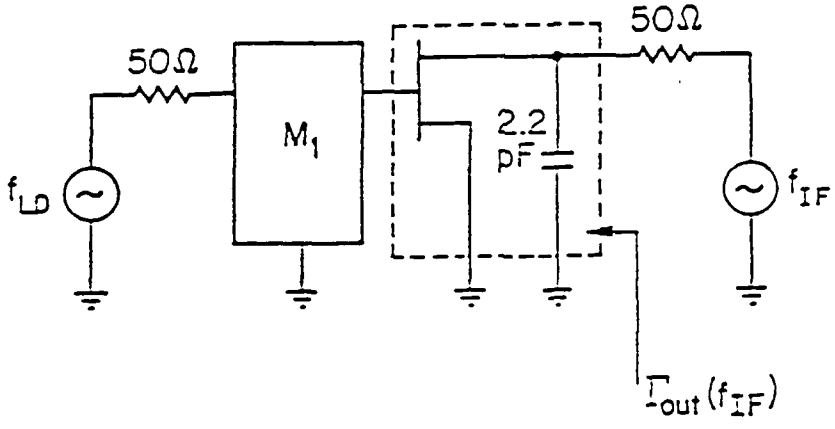

(b)

Figure 4.1(a),(b). Design procedures of a HEMT mixer

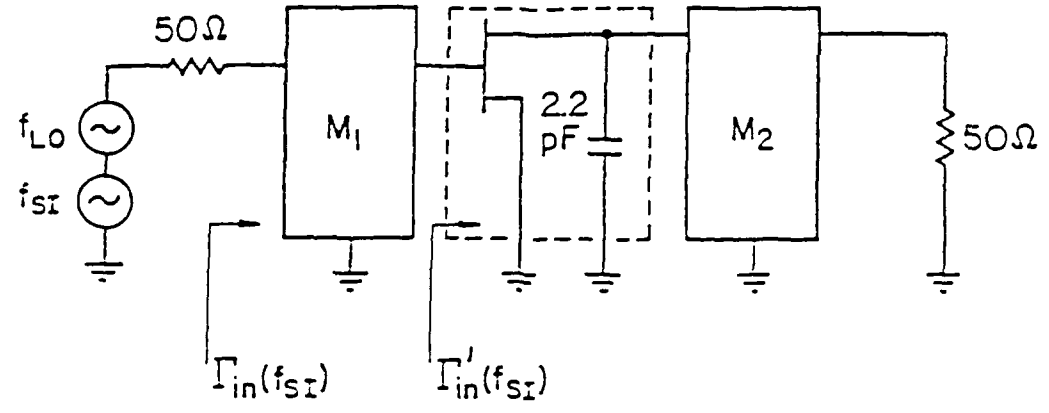

(c)

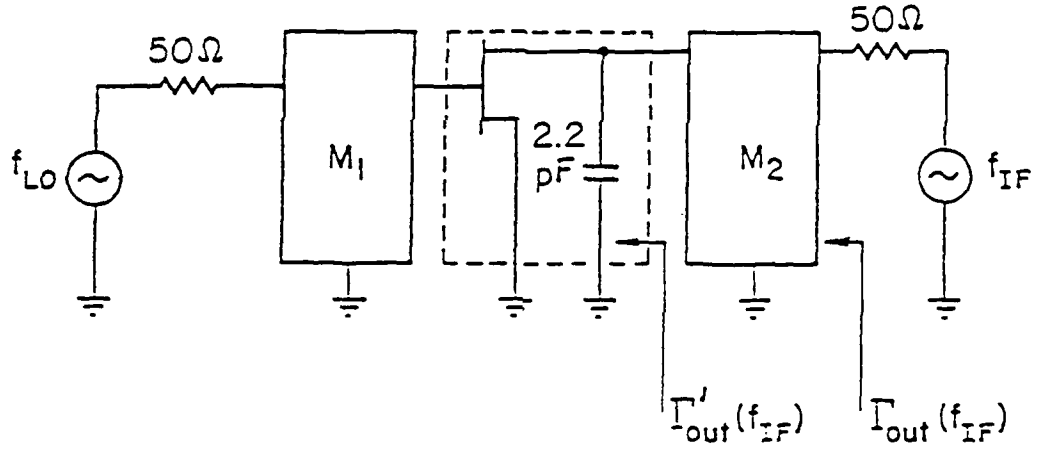

(d)

Figure 4.1(c),(d). Design procedures of a HEMT mixer

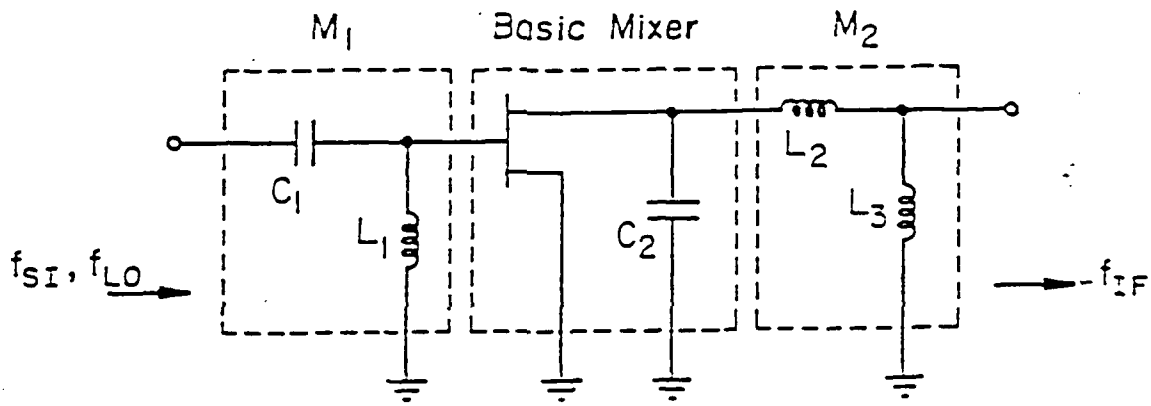

Figure 4.2. Circuit diagram of the HEMT mixer

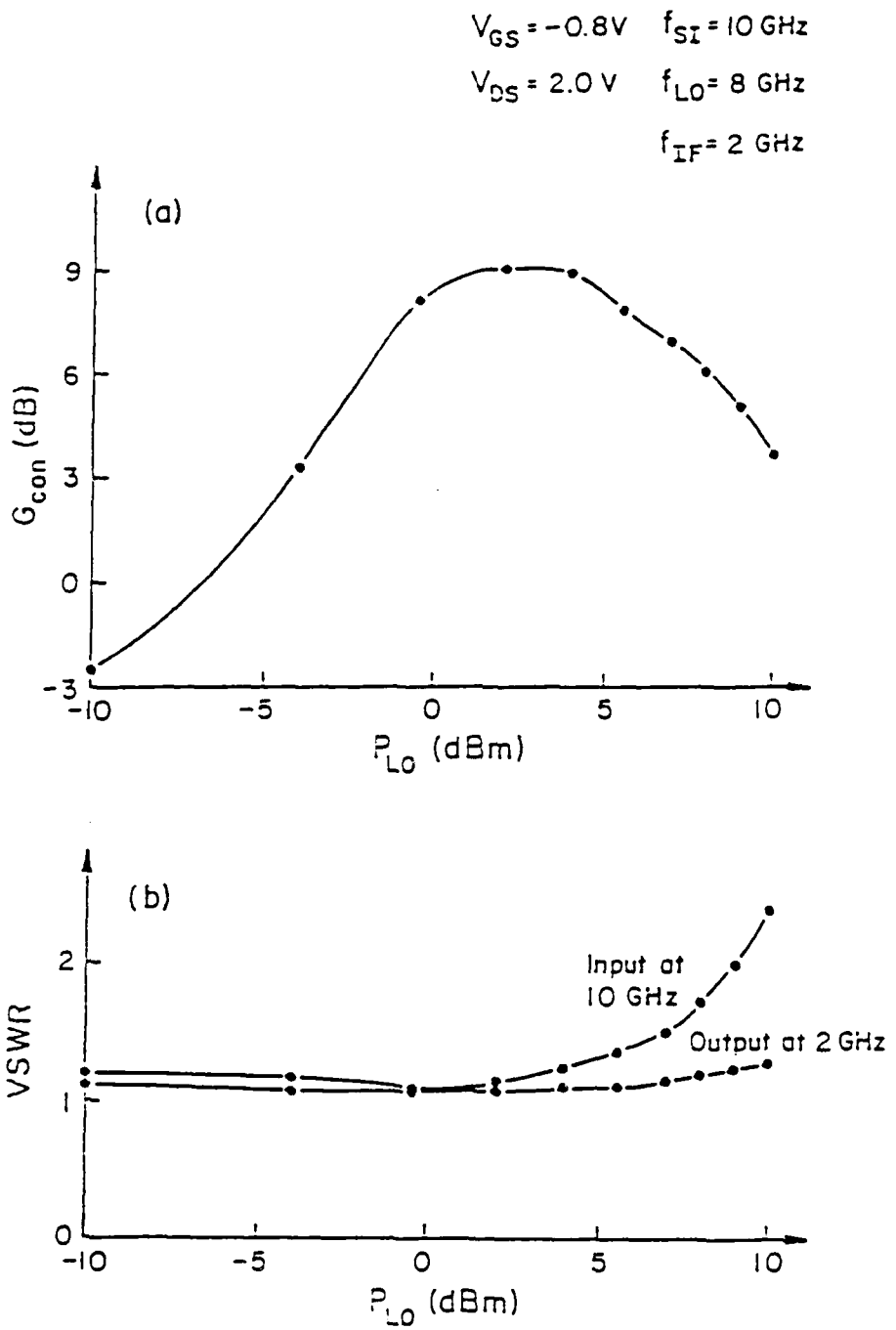

Figure 4.3. Performance of the 10 GHz mixer (a) conversion gain vs. LO power (b) VSWR vs. LO power

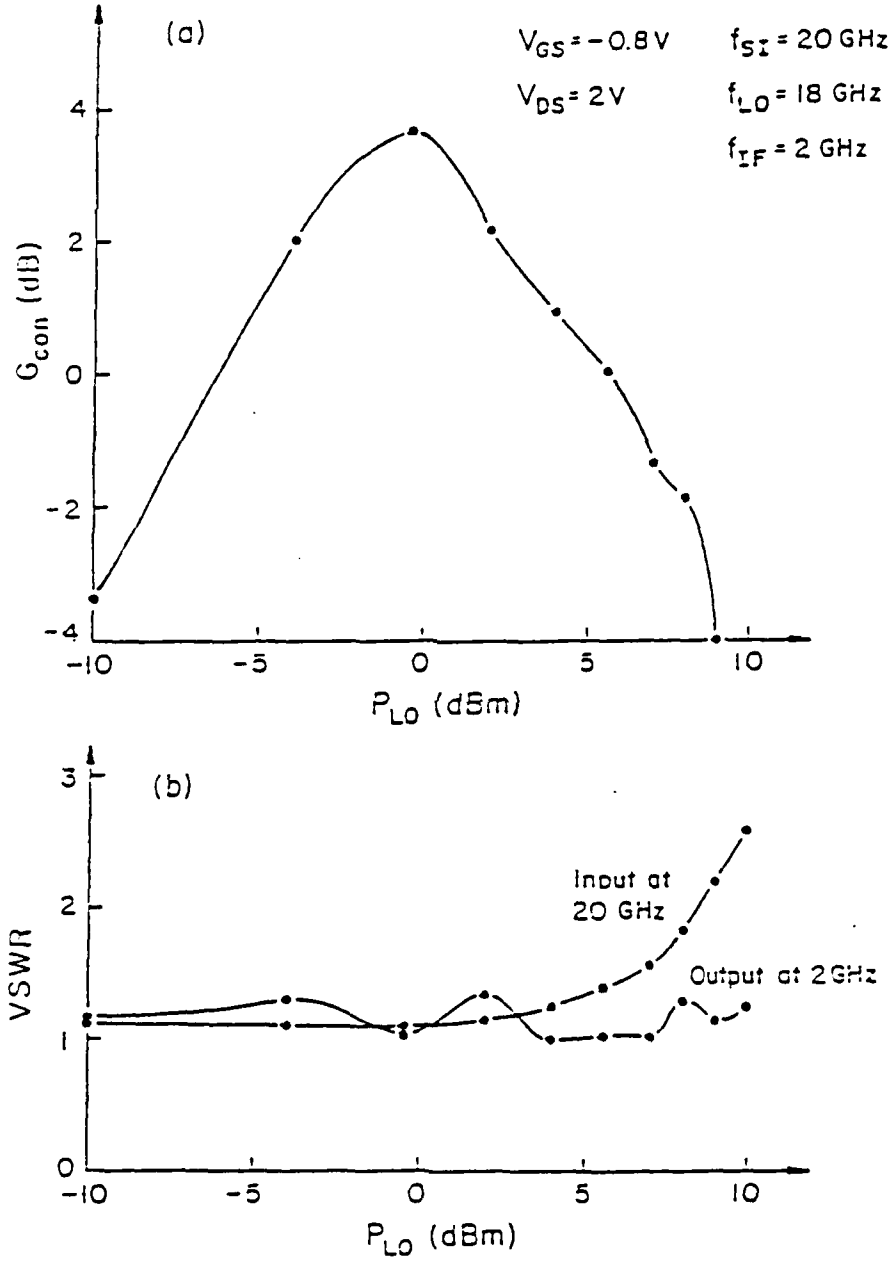

Figure 4.4. Performance of the 20 GHz mixer (a) conversion gain vs. LO power (b) VSWR vs. LO power

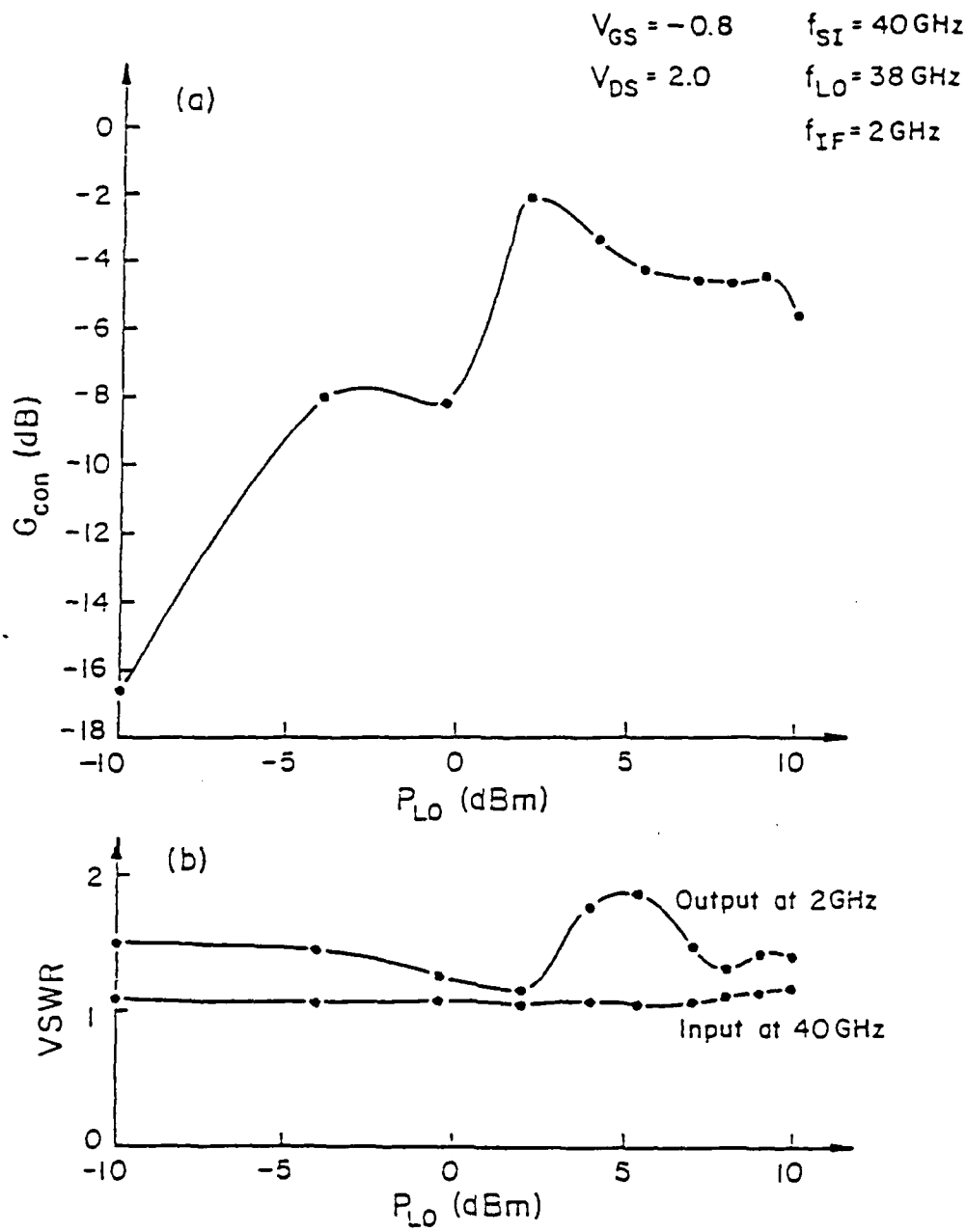

Figure 4.5. Performance of the 40 GHz mixer (a) conversion gain vs. LO power (b) VSWR vs. LO power

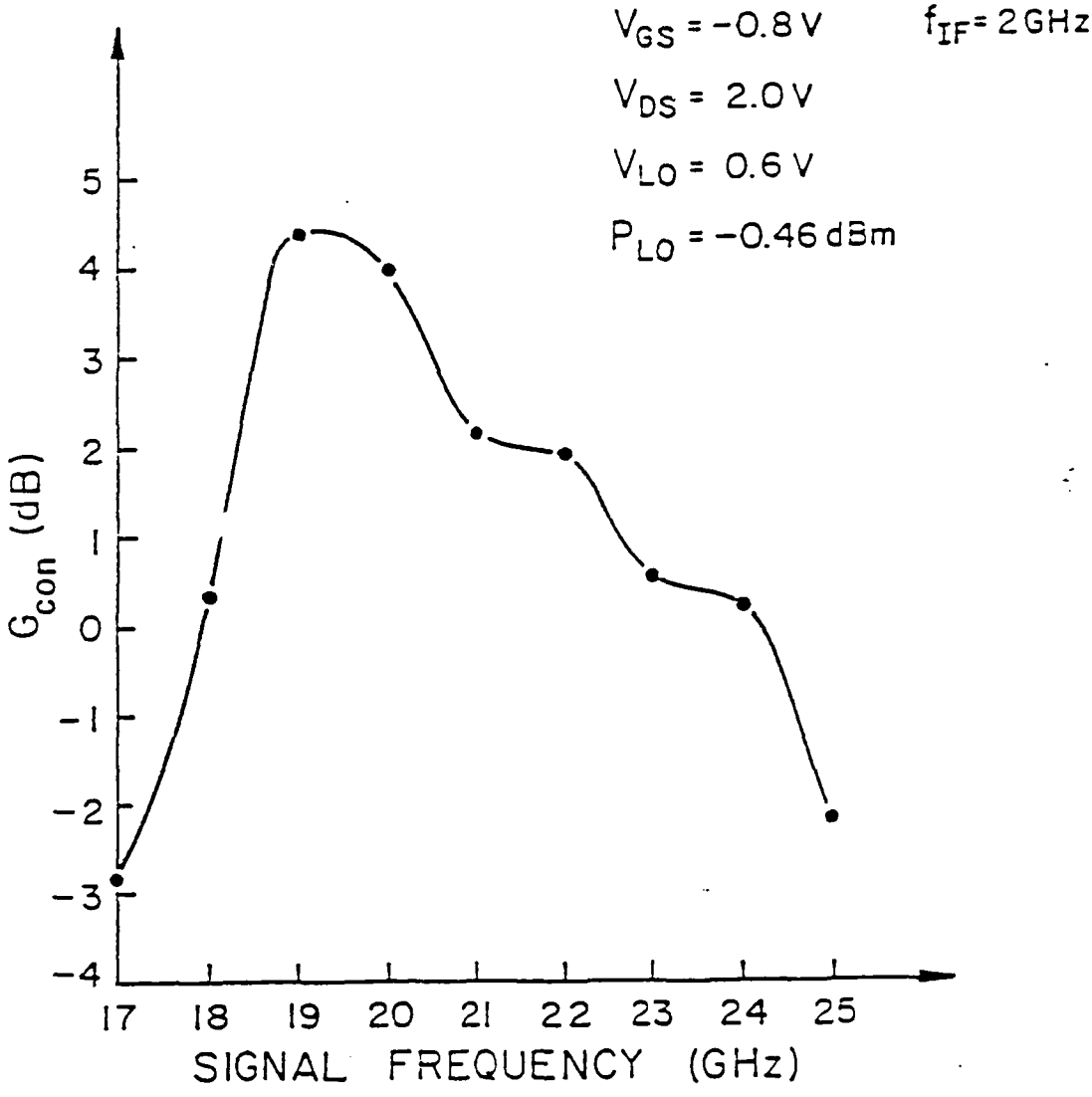

Figure 4.6. Frequency characteristics of the 20 GHz HEMT mixer

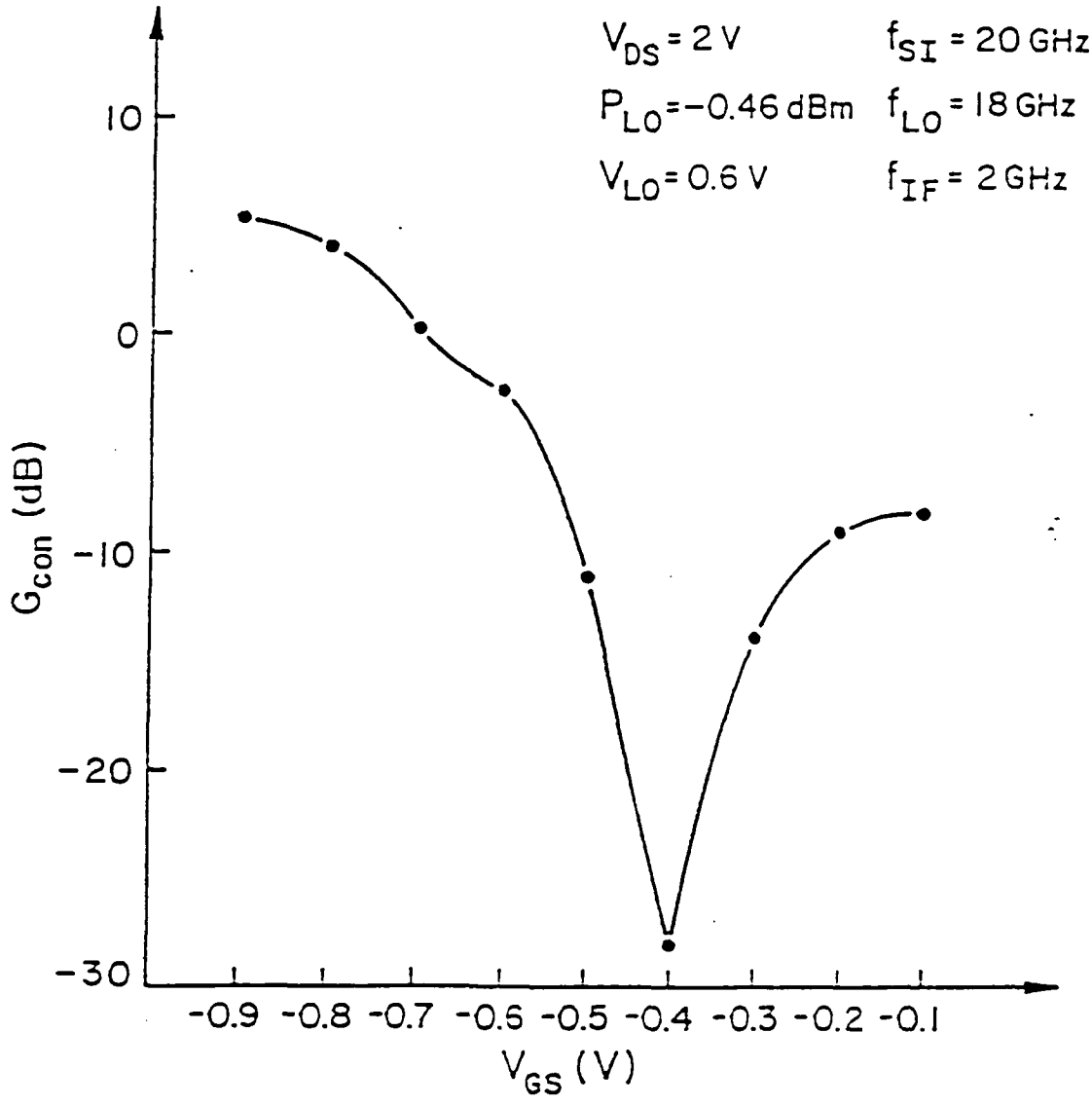

Figure 4.7. Conversion gain vs. gate bias of the 20 GHz HEMT mixer

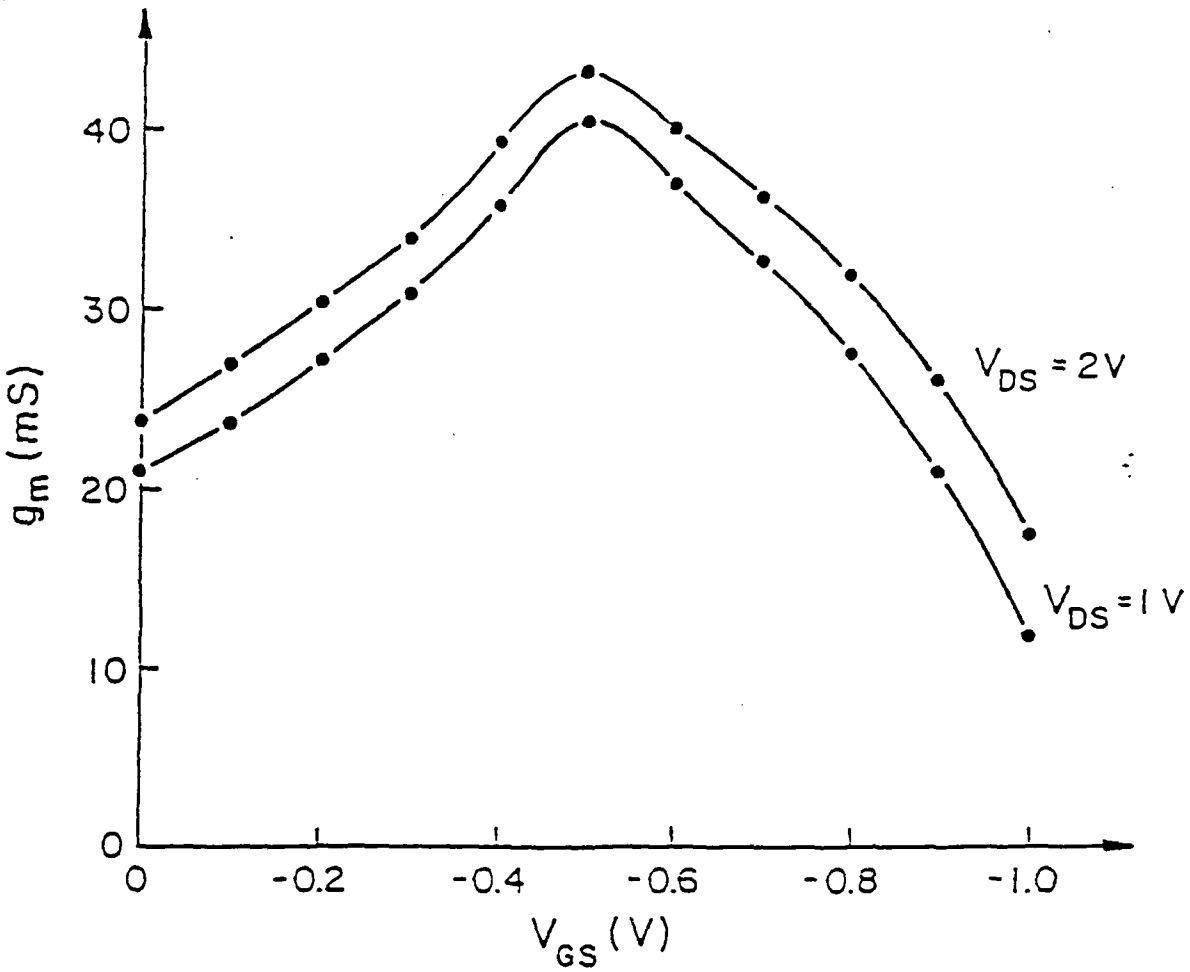

Figure 4.8. Transconductance vs. gate bias of the GE #5415 HEMT

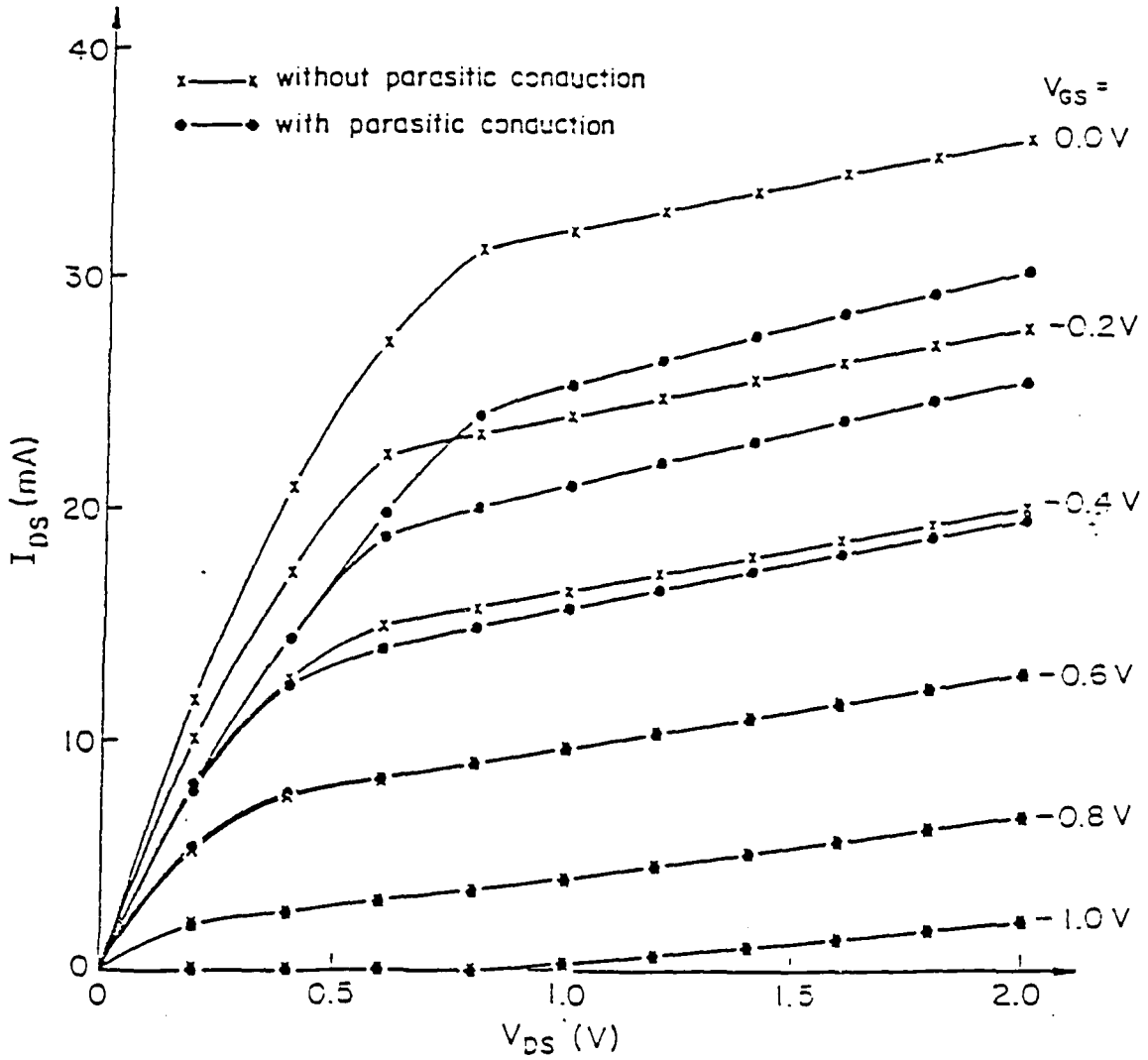

Figure 4.9. Comparison of the DC characteristics of the GE #5415 HEMT with and without transconductance compression

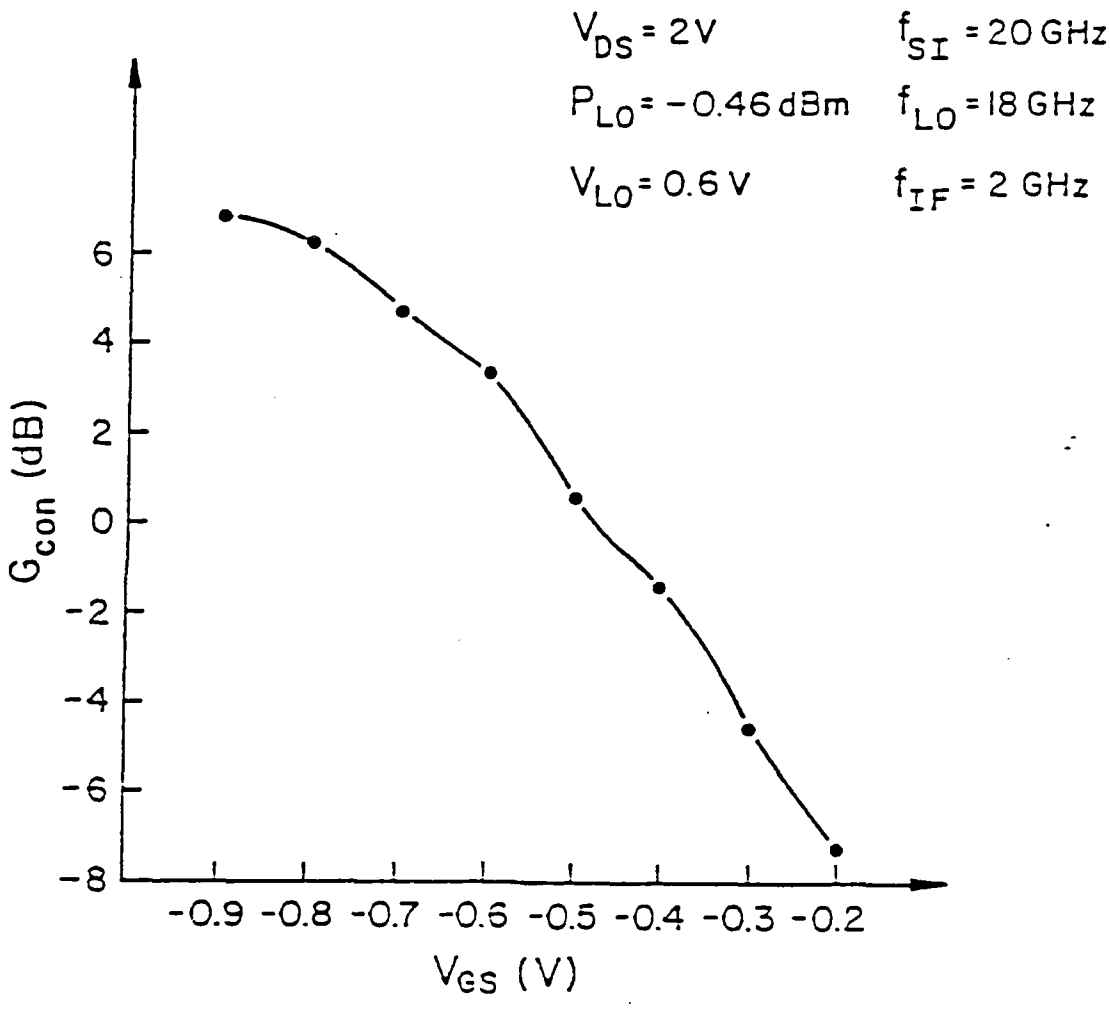

Figure 4.10. Conversion gain vs. gate bias of the modified HEMT mixer

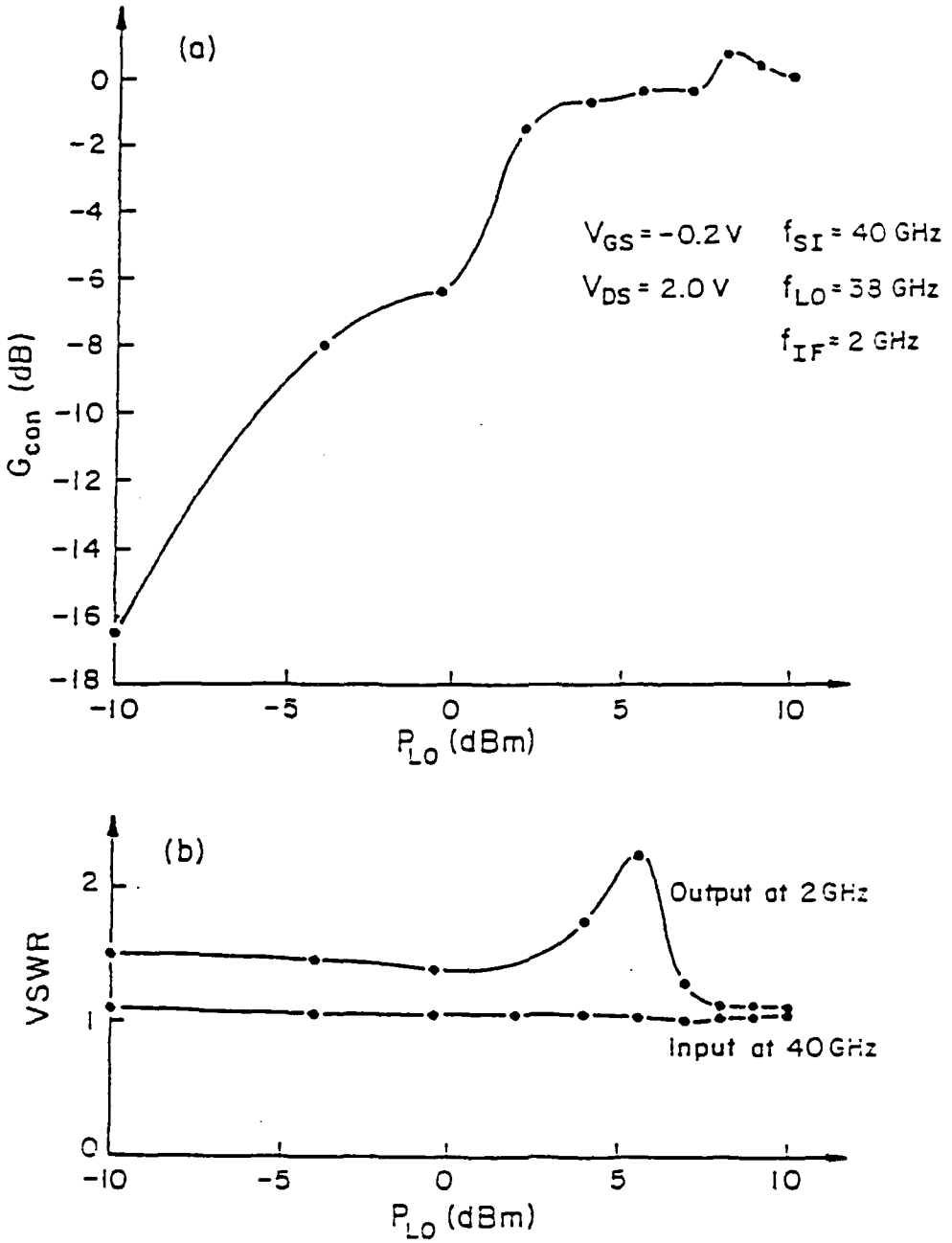

Figure 4.11. Performance of the 40 GHz mixer with modified GE HEMT
(a) Conversion gain (b) VSWR vs. LO power

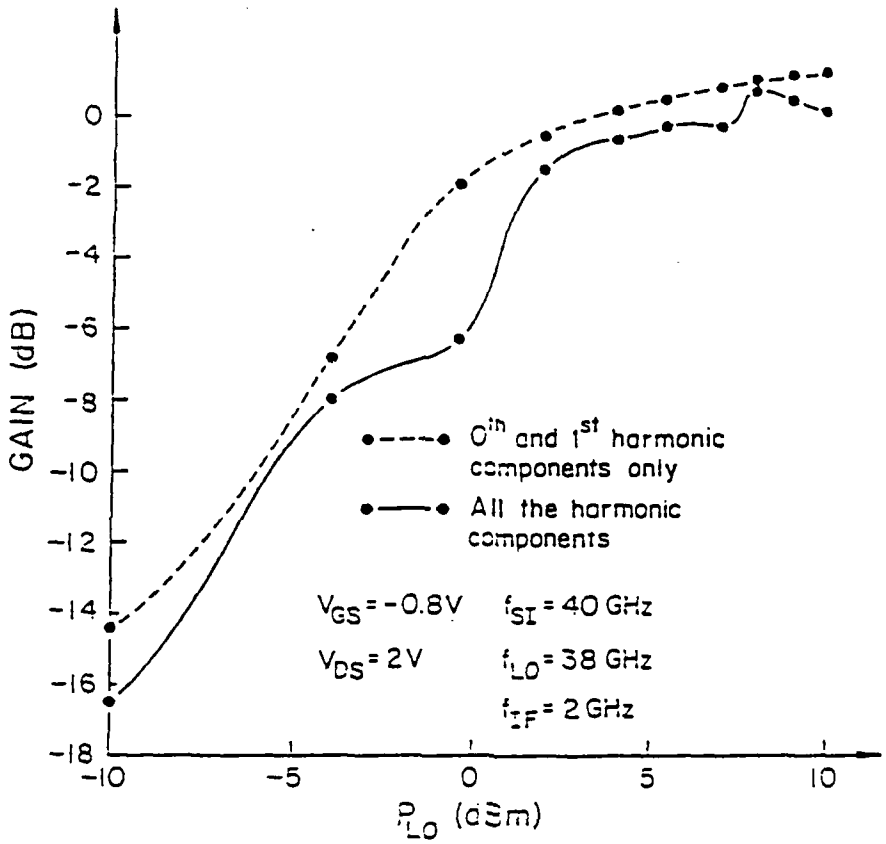

Figure 4.12. Comparison of the conversion gains of the 40 GHz mixer with the modified HEMT

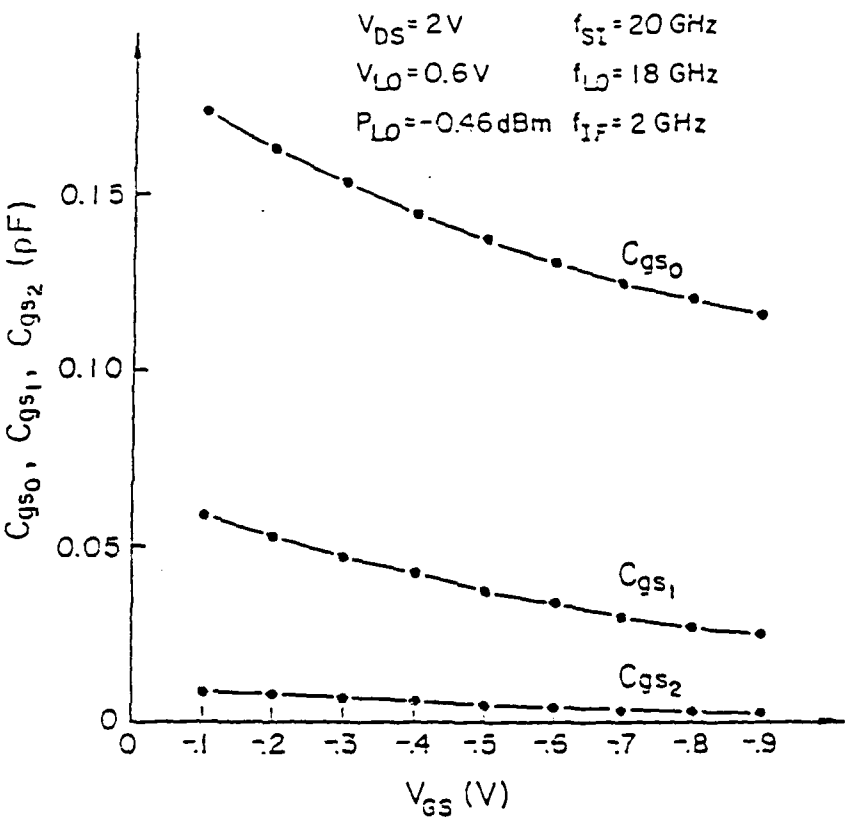

Figure 4.13(a). Fourier components of the gate capacitance vs. gate bias for the HEMT in 20 GHz mixer

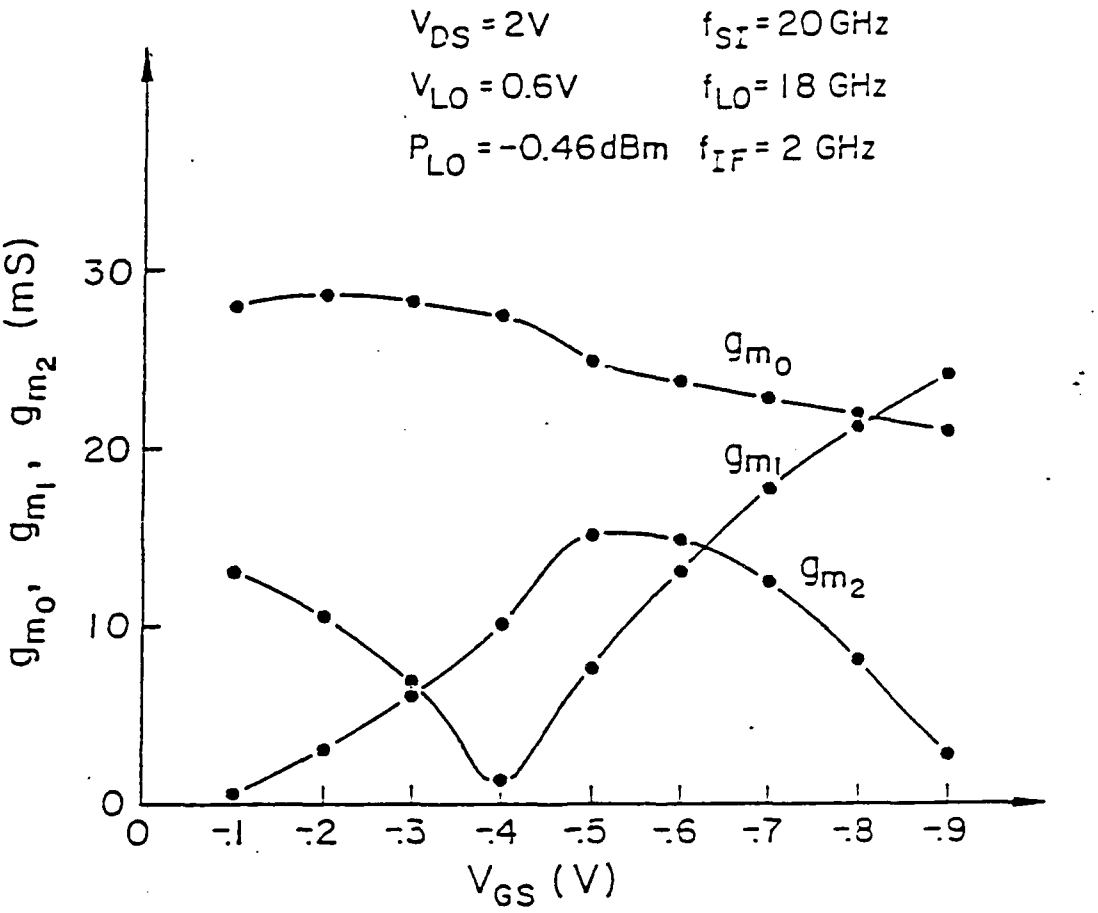

Figure 4.13(b). Fourier components of the transconductance vs. gate bias for the HEMT in 20 GHz mixer

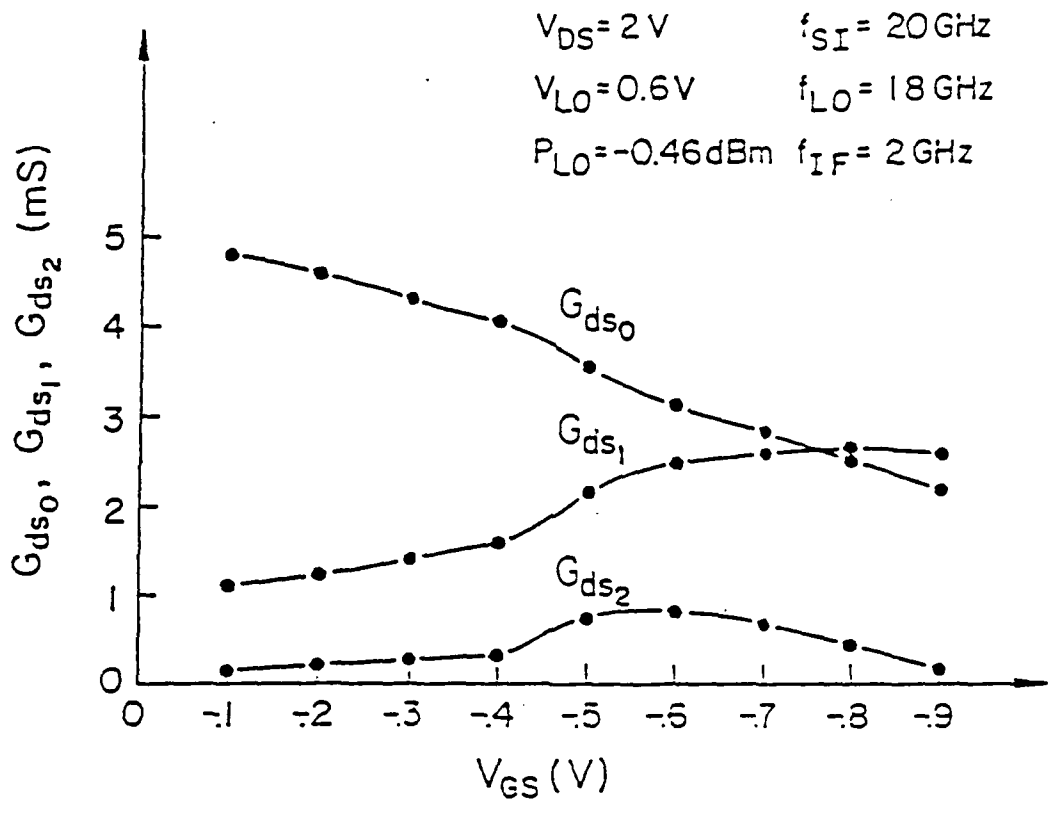

Figure 4.13(c). Fourier components of the output conductance vs. gate bias for the HEMT in 20 GHz mixer

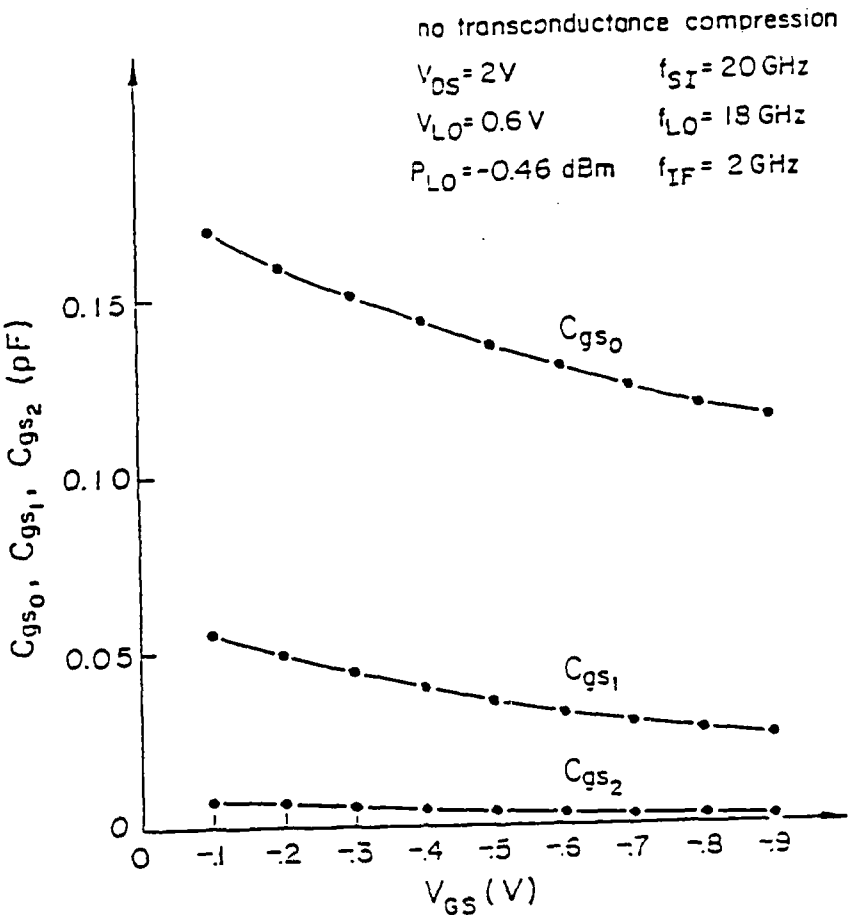

Figure 4.14(a). Fourier components of the gate capacitance vs. gate bias for the modified HEMT in 20 GHz mixer

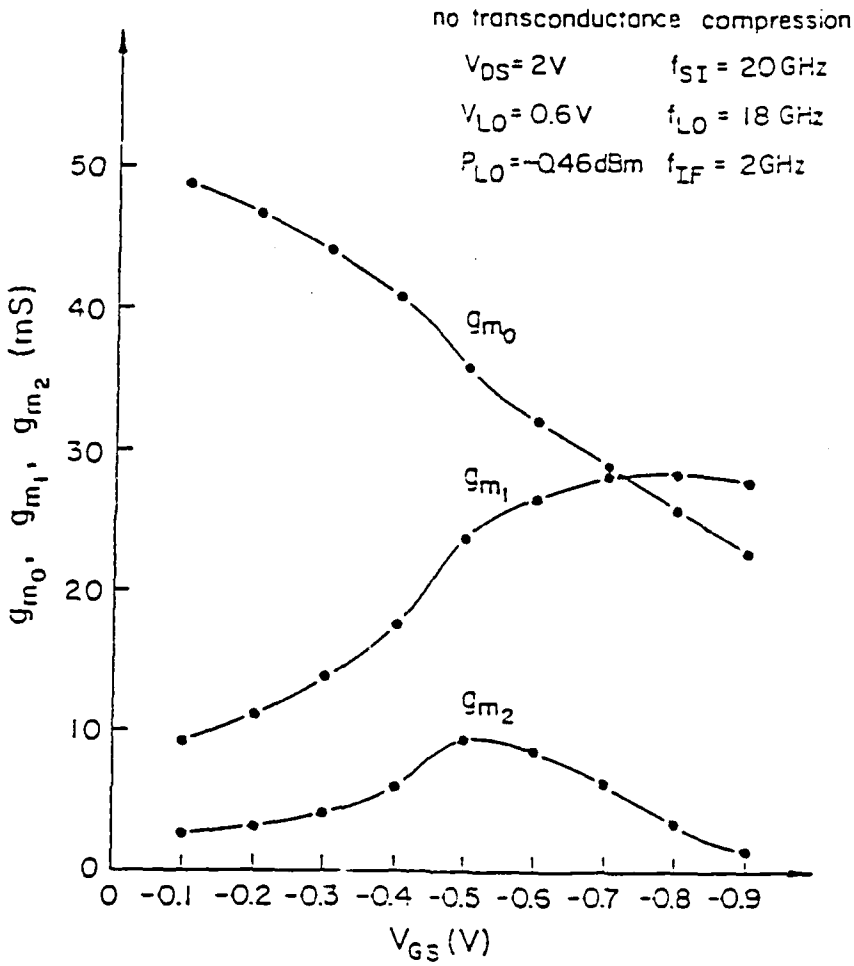

Figure 4.14(b). Fourier components of the transconductance vs. gate bias for the modified HEMT in 20 GHz mixer

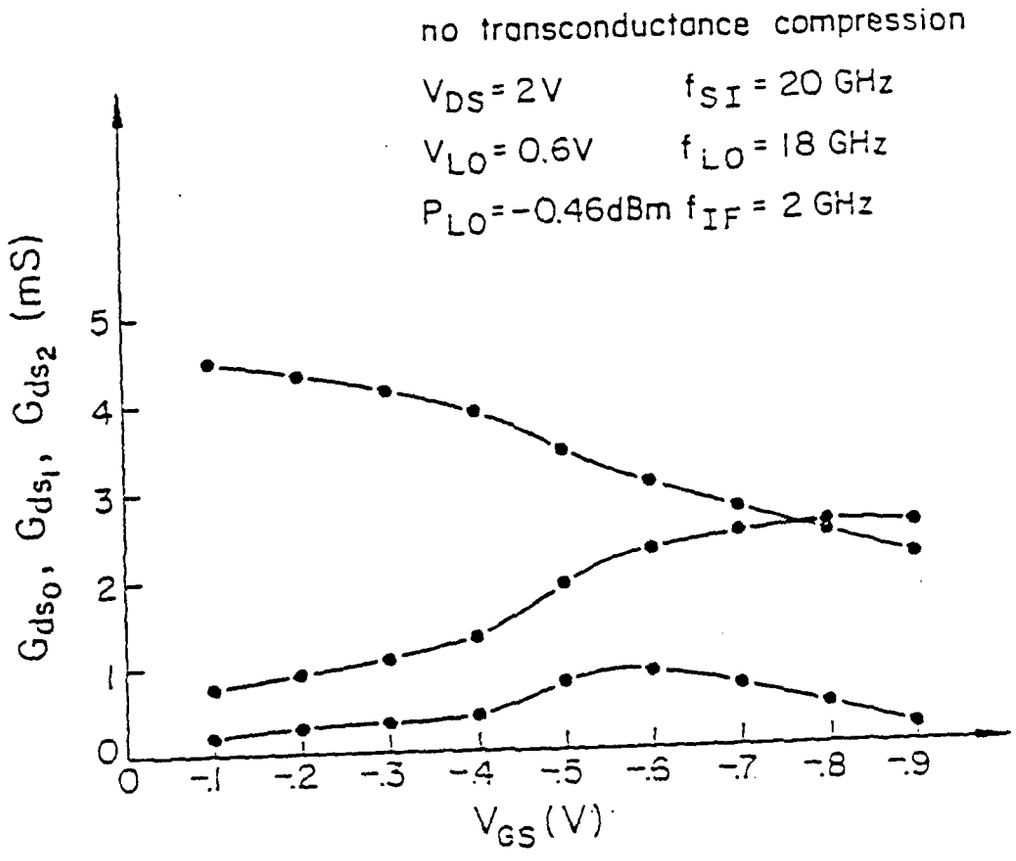

Figure 4.14(c). Fourier components of the output conductance vs. gate bias for the modified HEMT in 20 GHz mixer

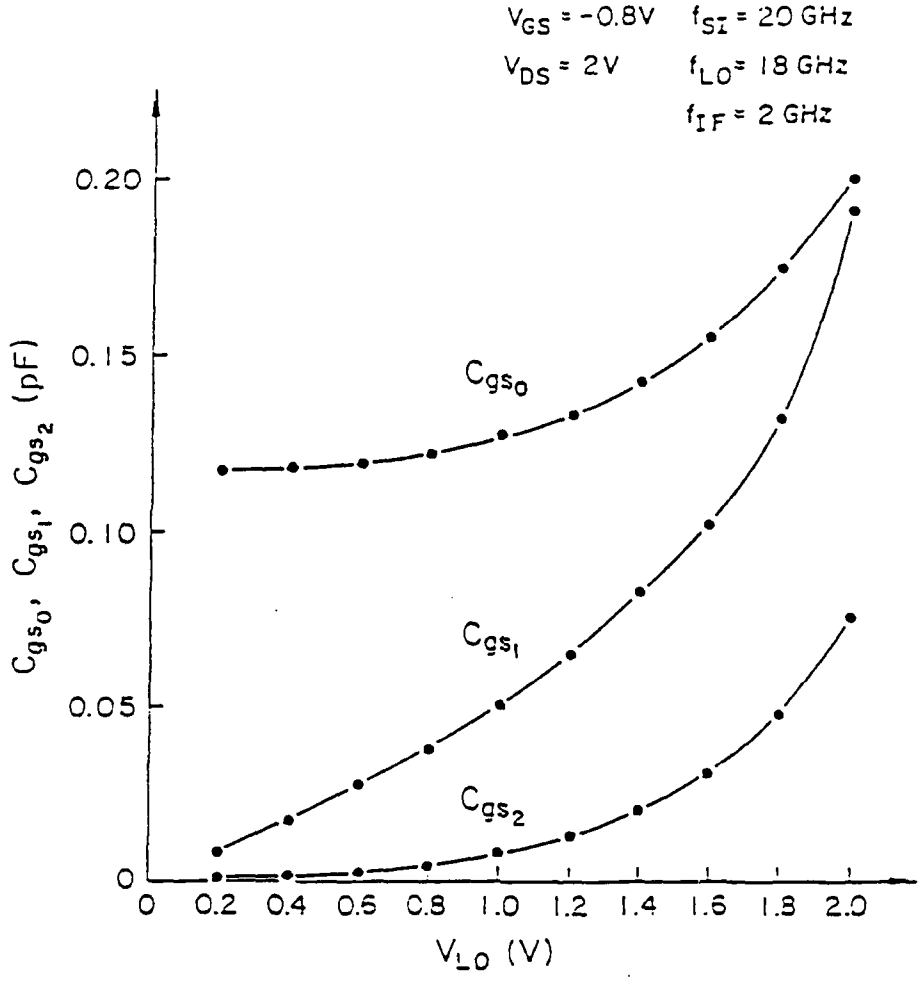

Figure 4.15(a). Fourier components of the gate capacitance vs. LO voltage for the HEMT in 20 GHz mixer

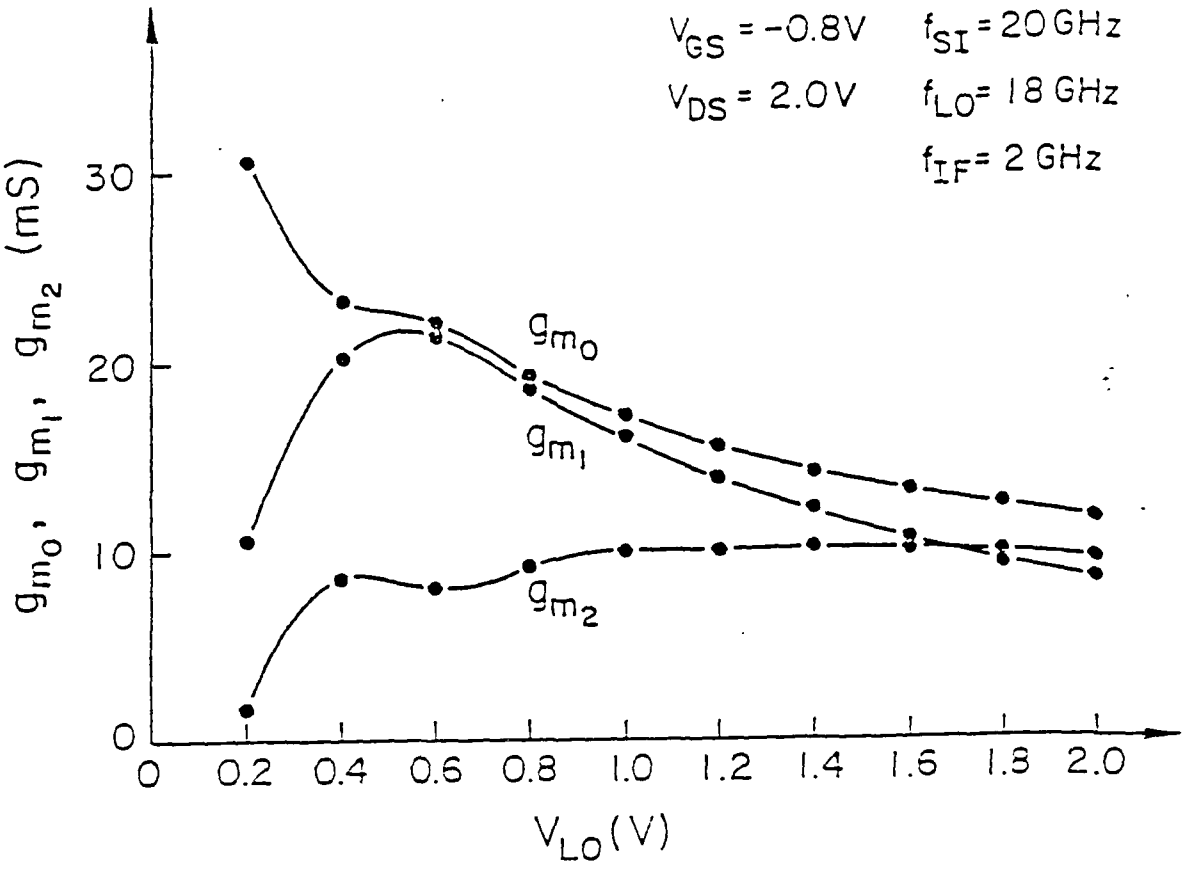

Figure 4.15(b). Fourier components of the transconductance vs. LO voltage for the HEMT in 20 GHz mixer

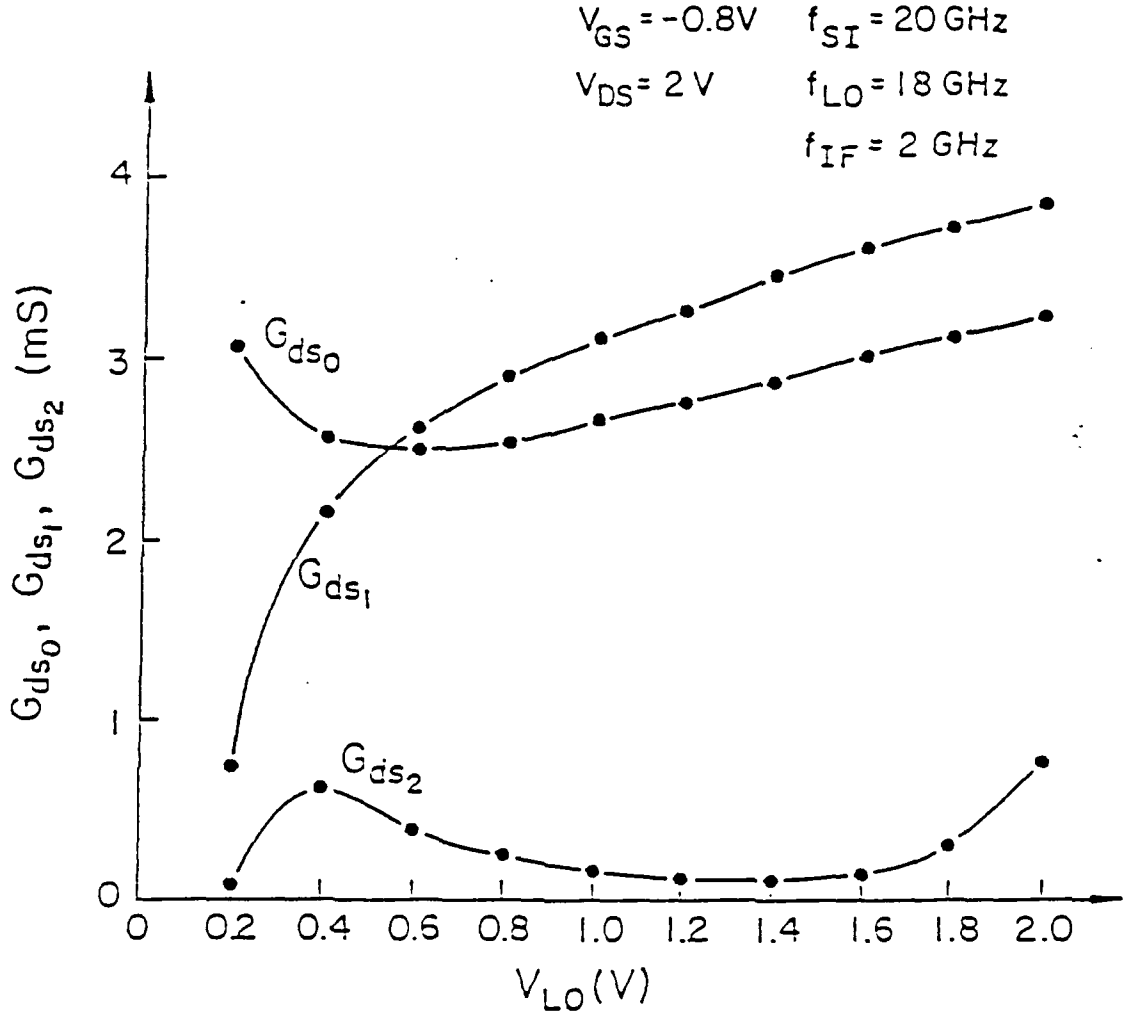

Figure 4.15(c). Fourier components of the output conductance vs. LO voltage for the HEMT in 20 GHz mixer

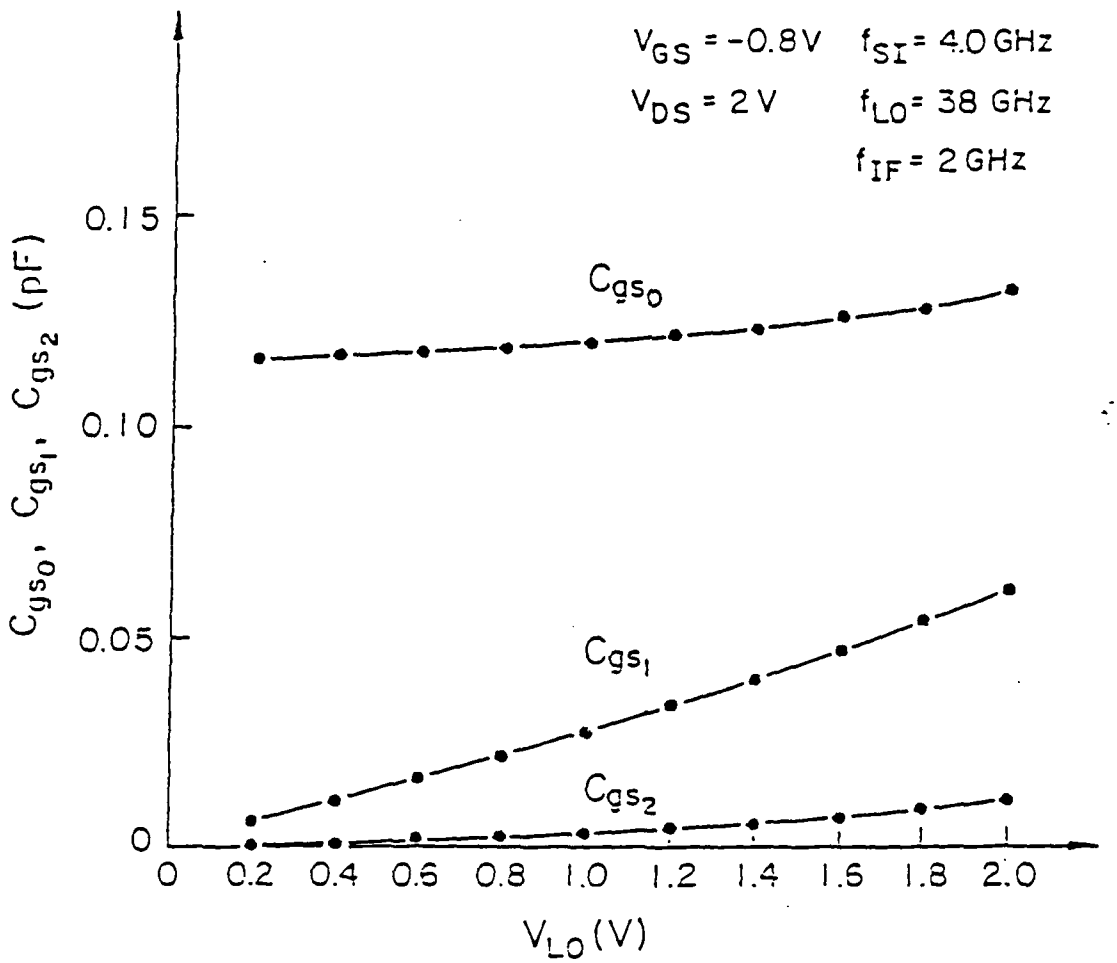

Figure 4.16(a). Fourier components of the gate capacitance vs. LO voltage for the HEMT in 40 GHz mixer

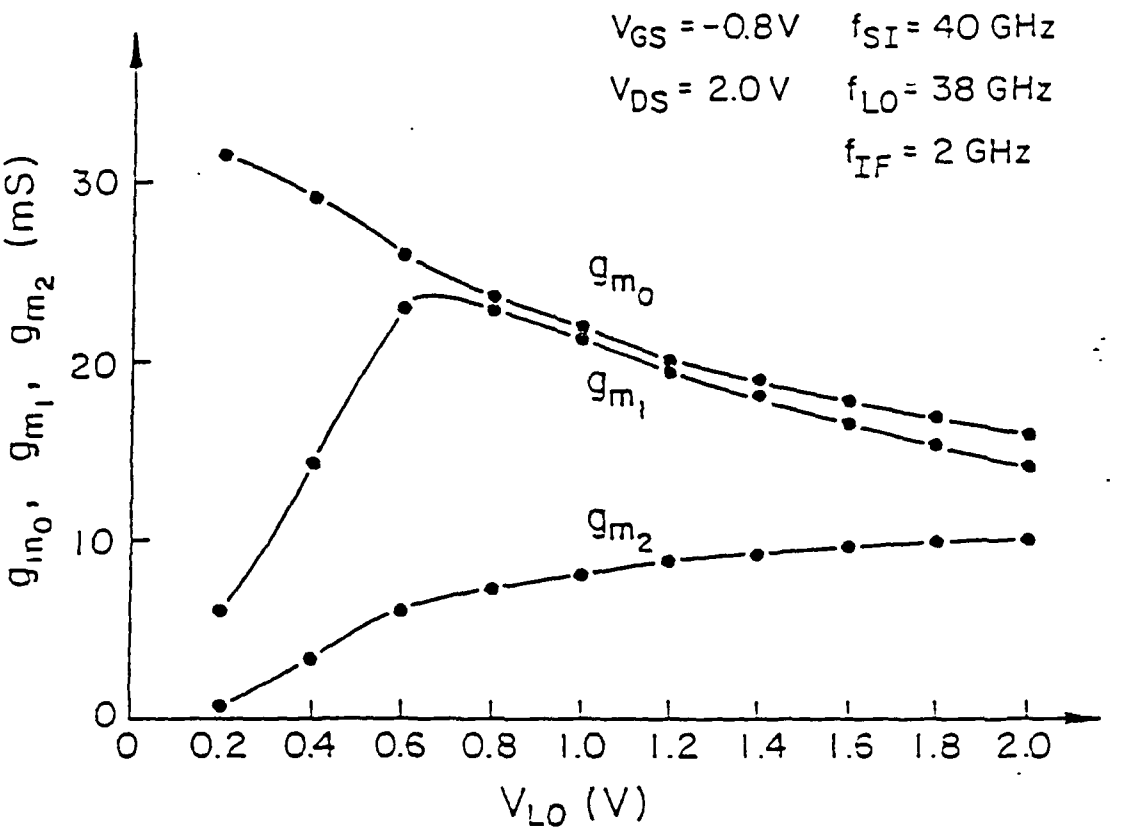

Figure 4.16(b). Fourier components of the transconductance vs. LO voltage for the HEMT in 40 GHz mixer

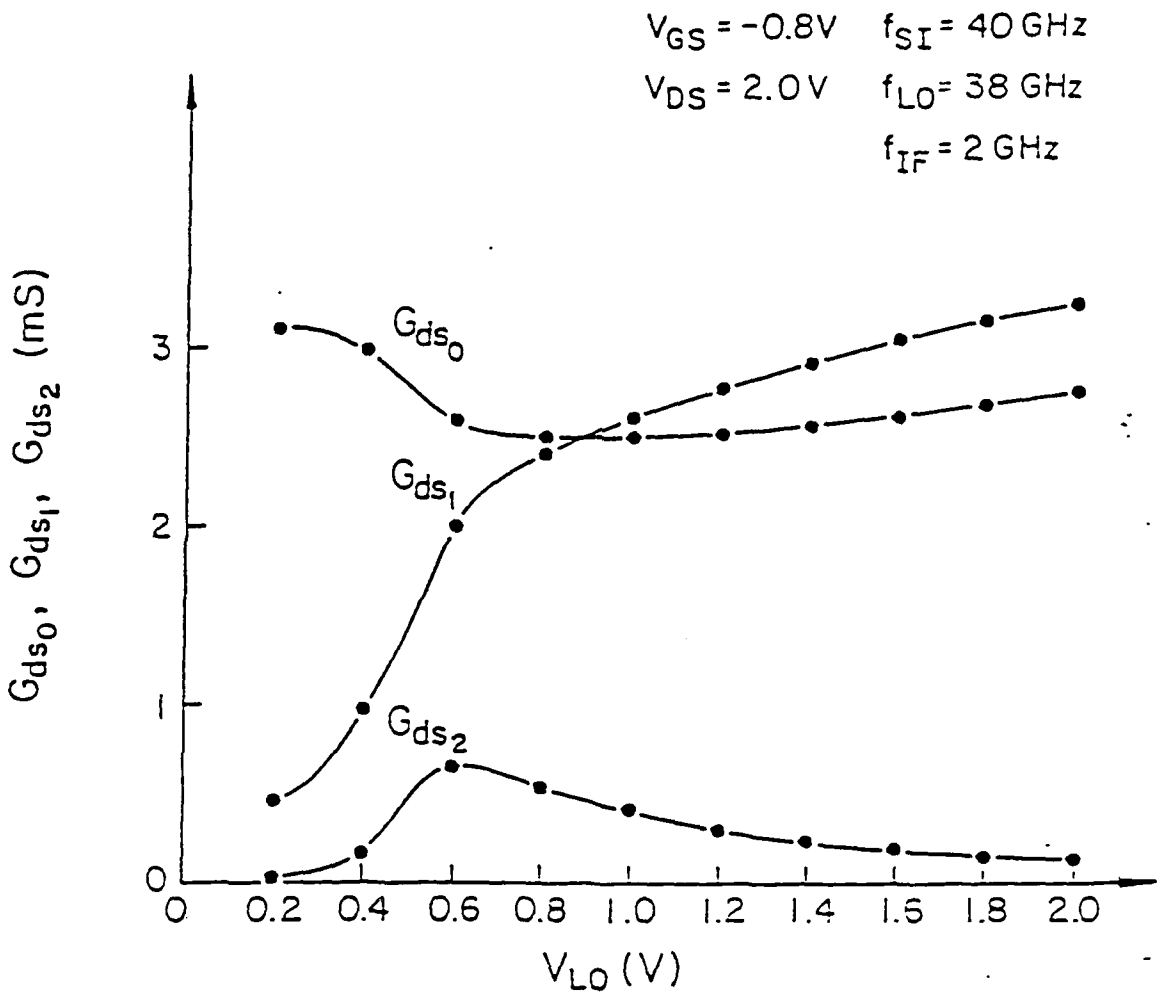

Figure 4.16(c). Fourier components of the output conductance vs. LO voltage for the HEMT in 40 GHz mixer

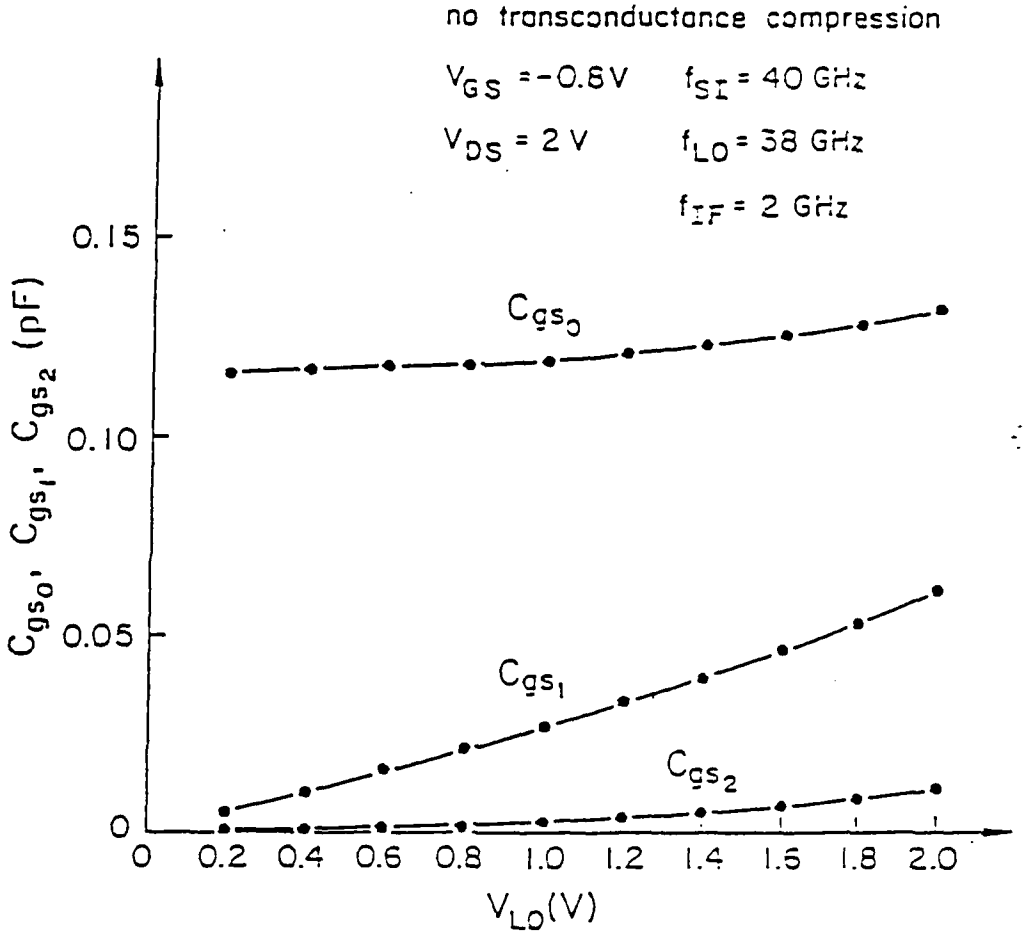

Figure 4.17(a). Fourier components of the gate capacitance vs. LO voltage for the modified HEMT in 40 GHz mixer

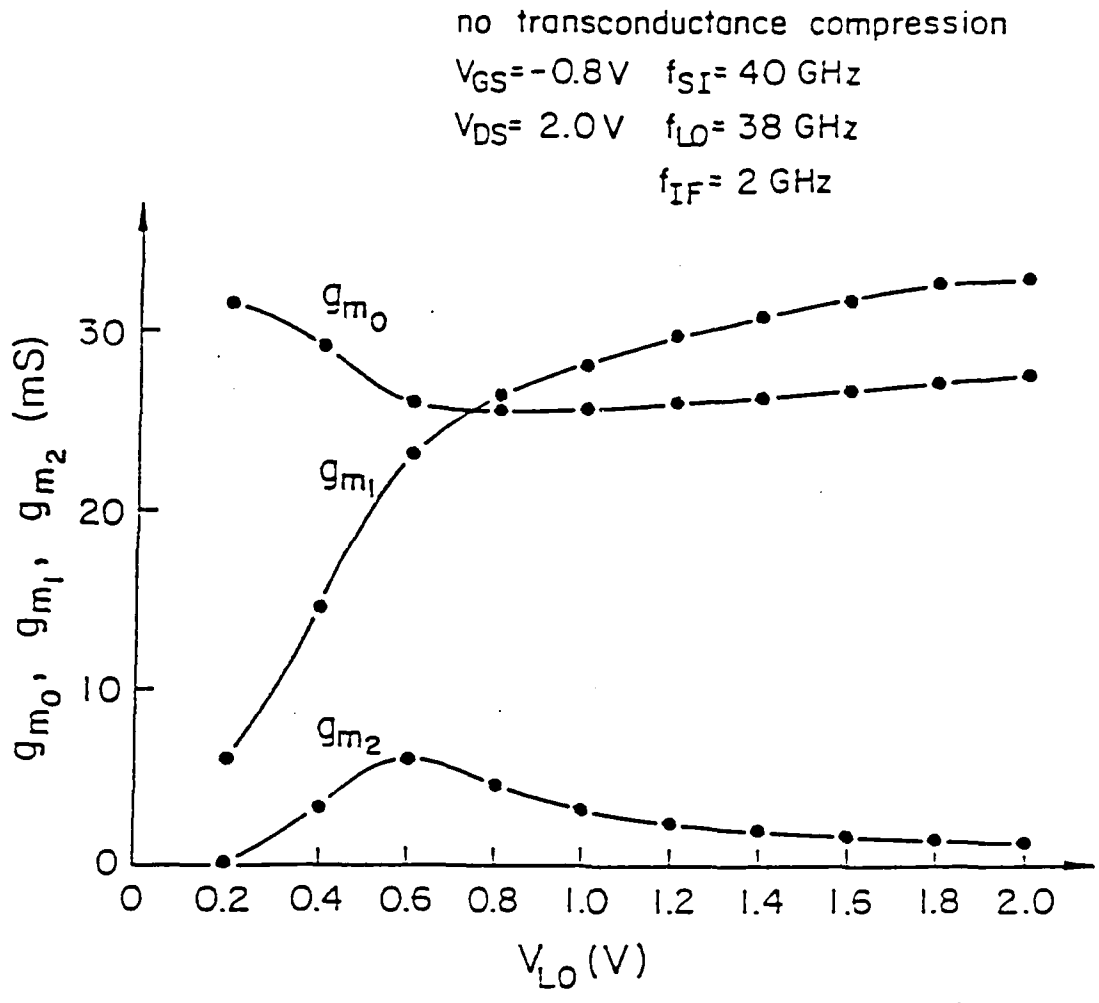

Figure 4.17(b). Fourier components of the transconductance vs. LO voltage for the modified HEMT in 40 GHz mixer

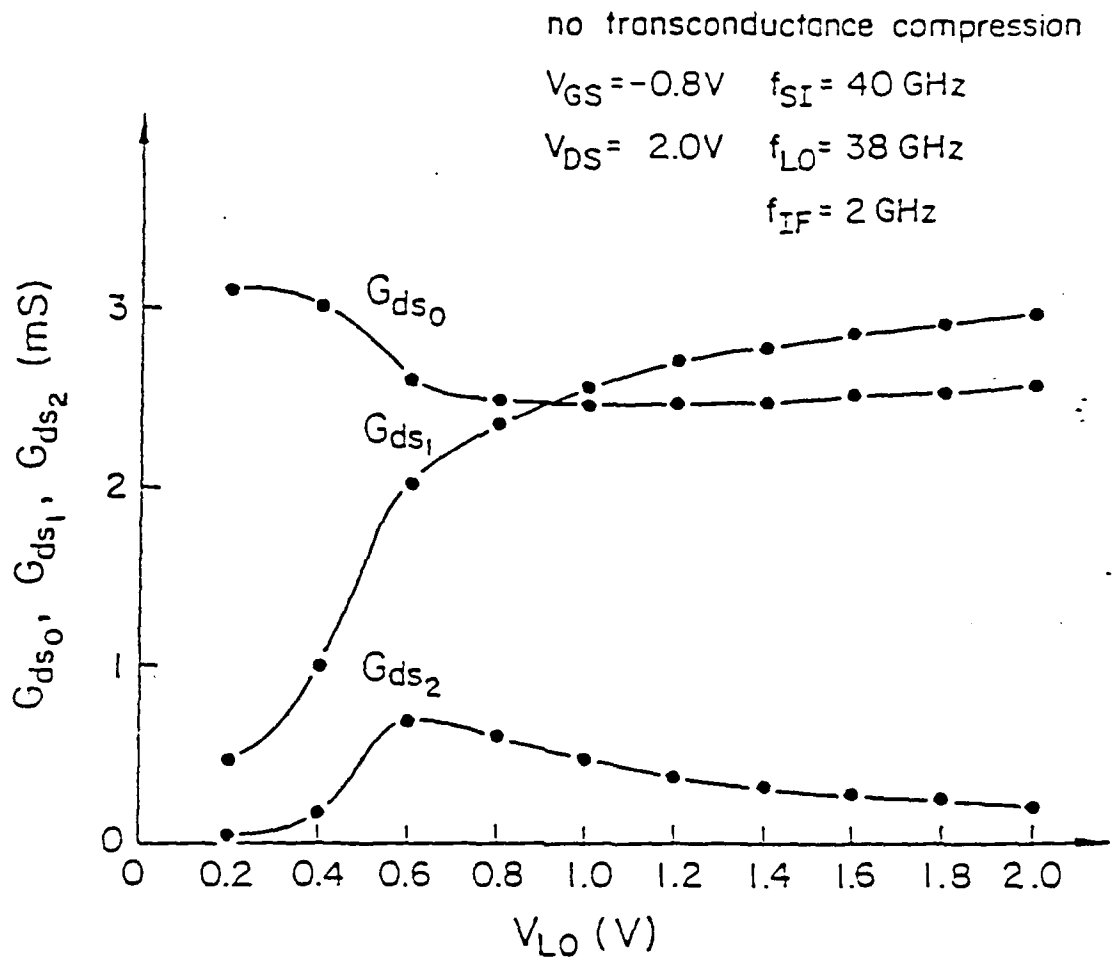

Figure 4.17(c). Fourier components of the output conductance vs. LO voltage for the modified HEMT in 40 GHz mixer

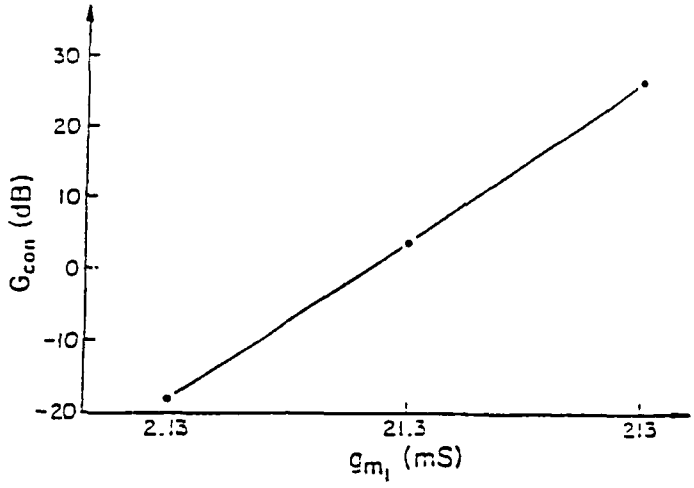
30
20
10
0
-10
-20
G_{con} (dB)
2.13
21.3
213
g_{m_1} (mS)

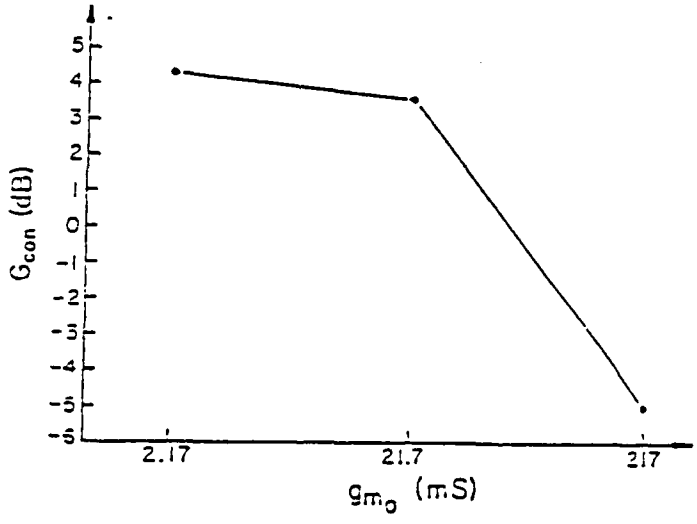
5
4
3
2
1
0
-1
-2
-3
-4
-5
-6
G_{con} (dB)
2.17
21.7
217
g_{m_2} (mS)

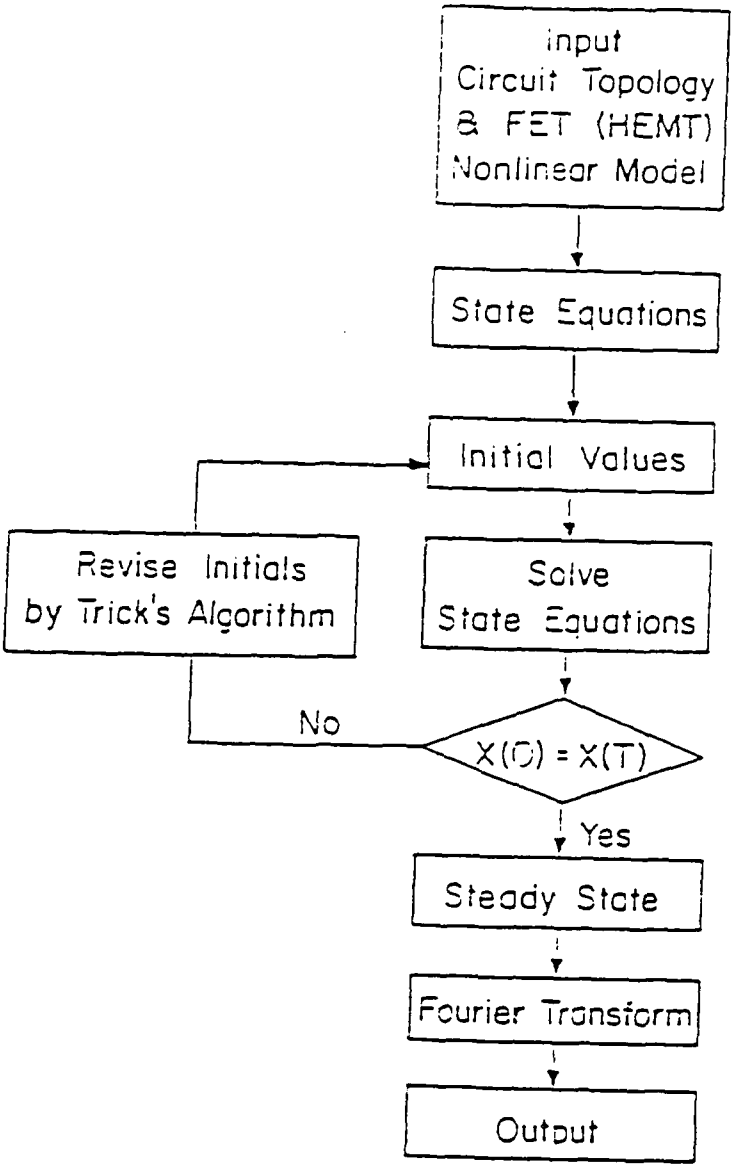

Figure A.1. Flow-chart of CADNON

Table 1(a) The Input File of the Lumped FET Mixer

```
; Time Domain Analysis of the Lumped FET Mixer Circuit
;
;       Circuit Elements
e 13 0 0.0 1.0 12.0 0.0
e 12 13 0.0 0.05 14.0 0.0
r 12 11 50.0
c 11 9 2.2
l 9 10 0.292
e 10 0 -3.5
l 9 7 0.15
l 7 6 0.206
r 6 5 2.6
c 5 4 0.438
r 4 2 1.75
c 5 3 0.03
j 3 2 5 4 m
c 3 2 0.081
r 3 2 560.0
l 3 8 0.2
r 2 1 100.0
l 2 1 0.035
r 1 0 3.85
c 8 0 2.2
l 8 14 1.769
l 14 15 1.04
e 15 0 3.0
r 14 0 50.0
;
;       FET Parameters
m 76.24 -4.274 0.726 0.295 0.143 0.065 0.5
;
;       Output Assignment
i r 1 0
v 14 0
v 5 4
z 11 0 r 12 11
;
;       Job-Consecution Parameters
1 2 2.0
1 2 2.5
```

Table 1(b)
Simulation Result of the Lumped FET Mixer Circuit

```
TIME DOMAIN ANALYSIS BY SHOOTING MODE

TIME-STEP ERROR TOL. = .10E-4    ST.-STATE ERROR TOL. = .50E-3
THE NUMBER OF TIME-STEPS = 300
THE NUMBER OF SAMPLING POINTS FOR ST.-TRAN. MTRX = 100

FUNDAMENTAL FREQUENCY = 2.00GHz

   ********** NEXT TASK **********

  E  13  0  0.0  2.5  12.0  0.0

(I R  1  0)
 0) 23.6856:    .0  1)   .2567: -63.0  2)  .0034:  76.0
 3)   .0002: -72.4  4)   .0005: -63.0  5)  .0133:  35.9
 6) 46.2667:  75.4  7)  1.2180:  27.4  8)  .0017: 172.7

(V 14 0)
 0)  3.0000:    .0  1)  .0347: 115.8  2)  .0001:-100.4
 3)  .0000: -79.0  4)  .0000:  -77.9  5)  .0001:  10.5
 6)  .0547:  55.6  7)  .0011:   -4.9  8)  .0000: -90.4

(V  5  4)
 0)  3.5912:-180.0  1)  .0005: 145.8  2)  .0000: -99.6
 3)   .0000:-171.5  4)  .0000: 161.1  5)  .0015:  30.8
 6)  2.7708:  27.1  7)  .0657: -24.1  8)  .0001: 137.1

(Z 11 0 R 12 11)
 0)  2.0803:    .0  1)560.8286: -21.5  2)  4.5546:-103.7
 3)  4.4838:-136.1  4) 18.4272: 164.1  5)==========:-140.2
 6)   .7230:  96.3  7)   .1985: -46.0  8) 45.0436: 130.3
```

Table 2(a)
The Input File of the Distributed FET Mixer

```
; Time Domain Analysis of the Distributed FET Mixer Circuit
;
;     Circuit Elements
e 12 0 0.0 2.5 12.0 0.0
r 12 11 50.0
c 11 9 2.2
r 9 10 0.005
t 10 13 70.0 0.12 100.0  14.0
r 13 14 0.005
e 14 0 -3.5
l 9 7 0.15
l 7 6 0.206
r 6 5 2.6
c 5 4 0.438
r 4 2 1.75
c 5 3 0.03
j 3 2 5 4 m
c 3 2 0.081
r 3 2 560.0
l 3 8 0.2
r 2 1 100.0
l 2 1 0.035
r 1 0 3.85
c 8 0 2.2
r 8 16 0.005
t 16 17 70.0 0.715 100.0 14.0
r 17 18 0.005
t 18 19 70.0 0.40  100.0 14.0
r 19 15 0.005
e 15 0 3.0
r 17 0 50.0
;
;     FET Parameters
m 76.24 -4.274 0.726 0.295 0.143 0.065 0.5
;
;     Output Assignment
i r 1 0
v 17 0
v 5 4
z 11 0 r 12 11
```

Table 2(b)
Simulation Result of the Distributed FET Mixer Circuit

```
TIME DOMAIN ANALYSIS BY HYBRID MODE

TIME-STEP ERROR TOL. = .10E-4    ST.-STATE ERROR TOL. = .50E-3
THE NUMBER OF TIME-STEPS = 1000
THE NUMBER OR SAMPLING POINTS FOR ST.-TRAN. MTRX = 50

NUMBER OF SECTIONS OF LINE (1) = 4
 LINE 1  DEL-L= .700E-01(NH)  DEL-C= .143E-01(PF)  DEL-R= .528E-01
NUMBER OF SECTIONS OF LINE (2) = 6
 LINE 2  DEL-L= .278E+00(NH)  DEL-C= .567E-01(PF)  DEL-R= .210E+00
NUMBER OF SECTIONS OF LINE (3) = 4
 LINE 3  DEL-L= .233E+00(NH)  DEL-C= .476E-01(PF)  DEL-R= .176E+00

FUNDAMENTAL FREQUENCY = 12.00GHz

(I R  1  0)
 0) 22.9903:    .0  1) 45.0042:  76.0  2)  20.2135:  30.8
 3)  4.2679:-176.3

(Z 11 0 R 12 11)
 0) 88.4421:-180.0  1)  .7128:  98.6  2)********:-131.6
 3)********: 127.2

(V 17  0)
 0)  2.9401:    .0  1)  .1272:  29.5  2)   .0601:-104.6
 3)   .0197:-153.9

(V  5  4)
 0)  3.5885:-180.0  1)  2.7076: 27.6  2)   .3127:-103.8
 3)   .0454: 177.0


    ****** PERTURBATION ANALYSIS ******

  VOLTAGE SOURCES
   NO.  FR TO    DC(V)   RF(V)   FREQ(GHz)
   1    12  0     .000   2.500   12.000
   2    14  0   -3.500    .000    .000
   3    15  0    3.000    .000    .000

  PERTURBATION SOURCES
     NO.  DC-AMP.  RF-AMP.  FREQ(GHz)
     1     .0000    .0500    14.000

     UPPER SIGNAL   FS= 14.000GHz   FL=12.000GHz
     OUTPUT ORDER ; 0)DC, 1)FS-FL, 2)2FL-FS, 3)FL, 4)FS

(I R  1  0)
```

0) .000: .0 1) .3059: -57.5 2) .0618:-103.6
3) .000: 90.0 4) 1.3608: 27.0

(V 17 0)
0) .000: .0 1) .0301: 120.5 2) .0002: -70.6
3) .0000: 90.0 4) .0041: -39.1

(V 5 4)
0) .0000: .0 1) .0008: 143.1 2) .0003: 148.2
3) .0000: 90.0 4) .0679: -20.5

(Z 11 0 R 12 11)
0) 1.0000: 180.0 1)********: -90.0 2)********: -90.0
3) 1.0000: 180.0 4) .2321: -23.1

NON-LINEAR COMPORNENTS
NO. 1
CGS(PF) 0) .193E 00: 0. 1) .653E-01: 26.4 2) .103E-01: 37.4
GM(S) 0) .125E-01: 0. 1) .158E-01: 25.2 3) .114E-02: 14.8
GDS(S) 0) .835E-03: 0. 1) .123E-02: 30.8 2) .398E-03: 68.6

PERTURBATION SOURCES
NO. DC-AMP. RF-AMP. FREQ(GHz)
1 .0000 .0500 14.100

UPPER SIGNAL FS= 14.100GHz FL=12.000GHz
OUTPUT ORDER ; 0)DC, 1)FS-FL, 2)2FL-FS, 3)FL, 4)FS

(I R 1 0)
0) .000: .0 1) .3144: -43.1 2) .0553: -86.0
3) .000: 90.0 4) 1.3734: 25.0

(V 17 0)
0) .000: .0 1) .0267: 91.6 2) .0002: -51.9
3) .0000: 90.0 4) .0041: -41.6

(V 5 4)
0) .0000: .0 1) .0010: 166.1 2) .0005: 163.9
3) .0000: 90.0 4) .0672: -22.9

(Z 11 0 R 12 11)
0) 1.0000: 180.0 1)********: -90.0 2)********: -90.0
3) 1.0000: 180.0 4) .2238: -34.9